2017-01-01

Constraining Times Of Extension In The Southern Rio Grande Rift And Basin And Range Using Apatite And Zircon (u-Th)/he Thermochronology

Julian Biddle
University of Texas at El Paso, jmbiddle@miners.utep.edu

CONSTRAINING TIMES OF EXTENSION IN THE SOUTHERN RIO GRANDE RIFT AND BASIN AND RANGE USING APATITE AND ZIRCON (U-TH)/HE THERMOCHRONOLOGY

JULIAN BIDDLE

Master's Program in Geology

APPROVED:

Jason Ricketts, Ph.D., Chair

Jose Hurtado, Ph.D.

Elizabeth Anthony, Ph.D.

Chunqiang Li, Ph.D.

Charles Ambler, Ph.D.
Dean of the Graduate School

CONSTRAINING TIMES OF EXTENSION IN THE SOUTHERN RIO GRANDE RIFT AND BASIN AND RANGE USING APATITE AND ZIRCON (U-TH)/HE THERMOCHRONOLOGY

by

JULIAN BIDDLE, B.S.

THESIS

Presented to the Faculty of the Graduate School of

The University of Texas at El Paso

in Partial Fulfillment

of the Requirements

for the Degree of

MASTER OF SCIENCE

Department of Geological Sciences

THE UNIVERSITY OF TEXAS AT EL PASO

December 2017

Abstract

The Rio Grande rift and the Basin and Range are adjacent extensional domains that have evolved contemporaneously in western North America. Although the rift is often considered to be the easternmost boundary of Basin and Range extension, there is geologic and geophysical evidence that suggests the two are discrete provinces. Existing low-temperature thermochronologic data indicate that a period of synchronous extension occurred across the entire length of the rift from ~25-10 Ma. However, these studies were more focused on the northern and central sections of the rift, and thermochronologic data remains sparse in southern New Mexico. We collected rock samples from the footwalls of normal faults in seven mountain ranges across southern New Mexico and southeastern Arizona, and from these samples a total of 42 zircon (U-Th)/He and 23 apatite (U-Th)/He ages were obtained. A change in thermochronologic age vs. eU relationships is observed to the west of the Cookes Range and Florida Mountains and suggests different extensional styles in the region. The change coincides with a previously proposed boundary between the Basin and Range and Rio Grande rift. We propose a master detachment fault controlling low-angle faulting in the Basin and Range in southern New Mexico. The hypothesized detachment, along with the crustal and mantle structure beneath the southern Rio Grande rift, are consistent with the simple shear model of lithospheric stretching.

Table of Contents

List of Tables

List of Figures

Chapter 1: Introduction

The Rio Grande rift is one of the world's major continental rifts, extending more than 1,000 km from Colorado to Mexico. Although the time of rift initiation is somewhat unconstrained, changing patterns in sedimentation, magmatism, and style of deformation all suggest that by 32-30 Ma the region was subjected to early extension (Morgan et al., 1986), and rifting has continued until the Present (Berglund et al., 2012). Although the rift has been extensively studied and is perhaps the most thoroughly researched continental rift in the world, there remain fundamental questions regarding its origin and cause(s) of formation. Several competing models for the activation of the rift have been proposed. Some models suggest that Rio Grande rift extension is driven by mantle forces, either through large-scale mantle upwelling based on mantle tomography (Moucha et al., 2008) or small-scale mantle convection at the edge of the stable Great Plains province (van Wijk et al., 2008). Other models rely on crustal forces to drive extension, and include clockwise rotation of the Colorado Plateau (Hamilton, 1981; Chapin and Cather, 1994; Landman and Flowers, 2013), collapse of overthickened continental crust (Cordell, 1978; Eaton, 1986), and initiation of a transform setting along the western margin of the North American plate (Dickinson and Snyder, 1979; Baldridge et al., 2006). A recent model suggests that detachment of a piece of the Farallon plate beneath the Rio Grande region in New Mexico enhanced asthenospheric upwelling in the slab window. This created a N-S trending zone of extension along the weakened crust that developed into the Rio Grande rift (Ricketts et al., 2016).

In addition, the rift's relation to the adjacent Basin and Range Province remains poorly understood and debated. Some argue that the Rio Grande rift is a not a distinct structural feature and is simply part of the larger Basin and Range Province (e.g. Baldridge et al., 1984). Physiographically, the southern Rio Grande rift resembles the Basin and Range because extension

is more diffuse and affects a wider region. However, the southern Rio Grande rift in southern New Mexico can still be distinguished from the Basin and Range because it has higher heat flow, deeper basins with Neogene sedimentary fill, and an abundance of Quaternary faults (Seager and Morgan, 1979; Keller et al., 1990). Constraining the timing of extension across the southern Rio Grande rift – Basin and Range transition is therefore important for addressing a variety of structural questions related to the underlying driving forces causing extension, and for investigating the nature of the boundary separating the two structural domains.

Chapter 2: Background

2.1 Rio Grande Rift History

The Rio Grande rift is a region of lithospheric extension situated between the Basin and Range Province and Colorado Plateau to the west and the Great Plains to the east (Fig. 1). The rift extends roughly north-south from northern Colorado to northern Mexico, and has a distinctive structural style of asymmetrical half-graben basins bounded by normal faults (e.g. Chapin and Cather, 1994; Kelley and Chamberlin, 2012). Half-grabens are typically bordered by master normal faults that accumulate a majority of fault displacement and result in uplift of the footwall block, often exposing Precambrian crystalline rocks at the Earth's surface. Broad accommodation zones transfer strain between basins through strike-slip and oblique-slip faulting and folding (e.g. Chapin and Cather, 1994; Goteti et al., 2013). From northern Colorado to central New Mexico, the rift is a discrete, narrow feature that consists of interconnected basins that have widths less than ~80 km. South of the Socorro "constriction" (Kelley, 1952), the rift abruptly widens and its physical expression becomes more diffuse. Here, the rift consists of multiple adjacent basins that have a combined width of ~180 km.

Initial extension in the rift occurred during in the late Oligocene (ca. 32-30 Ma) (Morgan et al., 1986), beginning a major period of extension that lasted until about 18 Ma, and was characterized by low-angle normal faults and andesitic volcanism (Cordell, 1978; Morgan et al., 1986) A second extensional period occurred ~10-5 Ma, and is responsible for the modern geomorphology of the rift (Morgan et al., 1986). This second extension phase was characterized by high-angle faulting and basaltic volcanism (Morgan et al., 1986). Sporadic extensional activity has continued from the end of the Miocene to the present (Cordell, 1978).

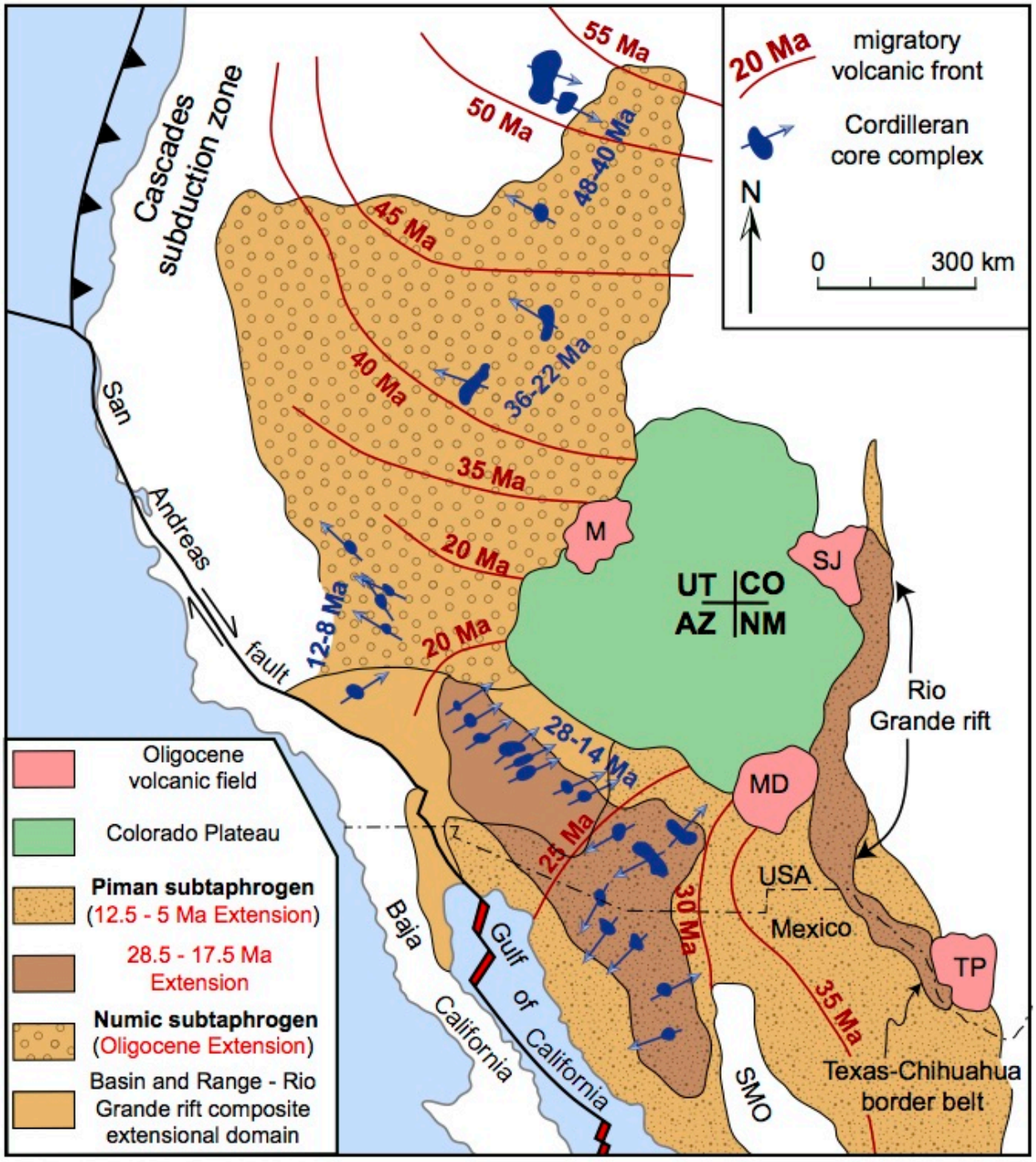

Figure 1: Regional tectonic map of the North American Cordillera. Extensional provinces and periods of magmatism and core complex formation are highlighted. M = Marysvale volcanic field; MD = Mogollon-Datil volcanic field; SJ = San Juan volcanic field; SMO = Sierra Madre Occidental; TP = Trans-Pecos volcanic field. UT- CO-AZ-NM is the Utah-Colorado- Arizona-New Mexico Four Corners junction. Map is modified from Dickinson (2002).

2.2 THERMOCHRONOLOGY STUDIES OF THE RIO GRANDE RIFT

Low-temperature thermochronologic data have been obtained for many of the uplifts associated with the central and northern portions of the Rio Grande rift in New Mexico and Colorado, including apatite fission-track (AFT) and apatite (U-Th)/He (AHe) datasets (Kelley et al., 1992; Kelley and Chapin, 1997; House et al., 2003; Landman and Flowers, 2013; Ricketts et al., 2015; 2016). The AFT method records when rocks cooled through temperatures of ~60-120 °C (Stockli, 2005), while the AHe method is sensitive to lower, yet overlapping, temperatures of ~30-90 °C (Flowers et al., 2009).

AFT studies from footwalls of master normal faults in Colorado and New Mexico record about 2-3 km of uplift and exhumation associated with rifting (Kelley et al., 1992; Kelley and Chapin, 1997; House et al., 2003). Cooling rates along the Rio Grande rift varied from 5-20 °C/Ma and increased over time (Kelley et al., 1992). Possible isothermal relaxation following increased volcanism in the Oligocene may have driven early cooling rates greater than 10° C/Ma along the eastern rift flank of the Albuquerque basin in central New Mexico (House et al., 2003). In the central and northern segments of the rift, AFT samples collected from the footwalls of major normal faults typically yield Neogene AFT ages, consistent with uplift and cooling due to extensional faulting during development of the Rio Grande rift. In contrast, Laramide AFT ages are preserved on the inactive half-graben margins, suggesting they were exhumed prior to extension in the rift. Recent studies have combined AFT and AHe data to constrain the low-temperature cooling history of rocks that were exhumed during rifting (House et al., 2003; Ricketts et al., 2016). In particular, Ricketts et al. (2016) use AFT and AHe constraints from the same samples to document a period of cooling from 25-10 Ma along the length of the Rio Grande rift from northern Colorado to southern New Mexico. These data do not support earlier models of rift

extension, which suggest two discrete periods of faulting from 32-18 Ma and from 10-5 Ma (Cordell, 1978; Morgan et al., 1986). The large number of ca. 25-10 Ma AFT and AHe ages coincides with a pause in magmatic activity in New Mexico and Colorado, suggesting that cooling during this time period was not likely related to Eocene-Oligocene large-volume magmatism. Instead, these ages most likely reflect cooling during simultaneous exhumation from normal faulting along most of the length of the entire rift (Ricketts et al., 2016). Preliminary AHe ages have also been collected as far south as the Franklin Mountains where the Rio Grande rift begins to physiographically blend with the Basin and Range Province (Delfin and Ricketts, 2016). These data suggest extension in the southern Rio Grande rift occurred simultaneously with the central and northern segments of the rift.

2.3 Basin and Range Province History

The Basin and Range province is a Cenozoic taphrogen (the extensional analogue of an orogen) along western North America that extends from southwest Canada to central Mexico (Fig. 1). The province is a composite domain composed of geodynamically distinct subtaphrogens (Dickinson, 2002). The region's characteristic geomorphology consists of systems of alternating horsts and grabens. Superextended crust resulting in denuded core complexes are also indicative of Basin and Range extension north of Mexico. The early phase of Basin and Range extension from the late Paleocene to middle Miocene occurred in isolated areas in northwestern North America and was caused by backarc basin processes from the subducted Farallon slab beneath North America (Eaton, 1982). Modern extension beginning ~17.5 Ma was driven by the initiation and evolution of the San Andreas transform fault (Nicholson et al., 1992; Dickinson, 2002). Extension generally swept from the north to the south across western North America over time, and was either concurrent with or postdated magmatic arc activity (Axen et al., 1993). The

southward sweep of magmatism has been associated with the steepening and ultimate foundering of the subducted Farallon slab beneath North America (Axen et al., 1993; Humphreys, 2009).

The Piman subtaphrogen of Dickinson (2002) is the southeastern section of the Basin and Range and includes southern Arizona as well as the Rio Grande rift (Fig 1) in New Mexico. In southeastern Arizona, core complex formation occurred from less than 30 to 12 Ma (Dickinson, 2002). The easternmost core complex was in the Pinaleño Mountains in southeastern Arizona, and was active until 19 Ma, based on geochronologic analysis of the core rock (Long et al., 1995). Widespread renewed crustal extension in the Piman started ~12.5 Ma, when the Rivera triple junction began migrating southward along the Pacific-North American plate boundary (Dickinson, 2002). Piman deformation largely ended at 6 Ma as extension began to be concentrated in the Gulf of California (Stock and Hodges, 1989; Staude and Barton, 2001). These times of extension in the southeastern Basin and Range echo the discrete periods of extension in the Rio Grande rift envisioned by early workers (Cordell, 1978; Morgan et al., 1986).

2.4 Difference Between the Southern Rio Grande Rift and Basin and Range Province

Although the Rio Grande rift in southern New Mexico and the Basin and Range are similar because they generally display diffuse extension, there is geologic and geophysical evidence that suggests the two are discrete provinces. The Rio Grande rift has more active Quaternary faults associated with deep rift basins that cut across Basin and Range faults (Seager and Morgan, 1979). Quaternary volcanism and higher heat flow are present across the rift, as well as positive gravity anomalies relative to the Basin and Range (Keller et al., 1990). The southern Rio Grande rift has a relatively thin crust that decreases in thickness from west to east, and contains a thickened mid-crust beneath the Potrillo Volcanic Field (Averill, 2007). Metamorphic core complexes,

characteristic of Basin and Range extension, are absent from the Rio Grande rift, although there is evidence of early-stage core complex development in the central rift (Ricketts et al., 2015). These differences suggest that the Rio Grande rift is a distinct structural entity from the Basin and Range, and the two may have evolved separately from other, possibly in response to different driving forces. There have been two boundaries proposed between the provinces in southern New Mexico (Fig. 2). The first possible boundary is located to the west of the Cookes Range and the Florida Mountains (Woodward et al., 1978; Keller et al., 1990), while the second is east of these ranges (Seager and Morgan, 1979; Mack, 2004).

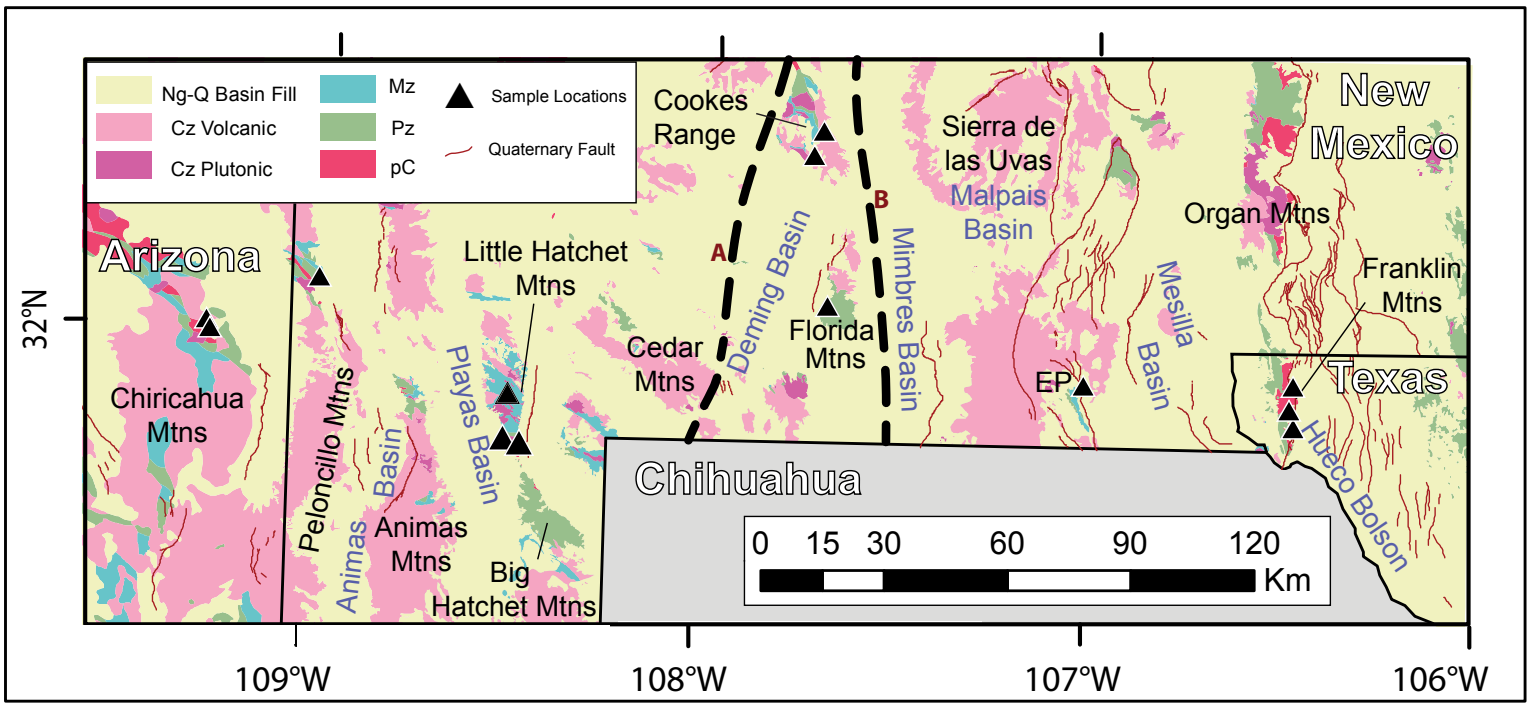

Figure 2: Study area. Dashed lines A (Woodward et al., 1979) and B (Mack, 2004) represent possible boundaries between the Basin and Range and Rio Grande rift.

Chapter 3: Thermochronologic Methods

To add to the wealth of thermochronologic data in the northern and central segments of the rift, and to compare to the times of extension in the Basin and Range Province, rock samples were collected from the southern New Mexico region where the two structural features merge (Fig. 2). Rocks were collected in the footwalls of major basin-bounding normal faults. The purpose of this careful sample collection was to collect samples immediately adjacent to faults because these rocks are most likely to record exhumation during faulting, and therefore can be used to document times of faulting. For most samples, we obtained AHe and zircon (U-Th)/He (ZHe) data to tightly constrain each samples' low-temperature cooling history from approximately 200 °C to near-surface temperatures.

3.1 Apatite (U-Th)/He Thermochronology

AHe makes use of the (U-Th)/He radioisotopic dating system. It involves the radioactive decay of ^{238}U, ^{235}U, and ^{232}Th into Pb isotopes, by expulsion of alpha particles. The positively charged alpha particles are ejected at high velocity through a crystal lattice but due to interactions with lattice atoms, they eventually stop and become electrically neutral (Tagami and O'Sullivan, 2005). The now neutral alpha particles are identical to ^{4}He. The ages of apatite minerals can thus be found by comparing the amounts of U and Th to the accumulated He and knowing the decay constant for each parent isotope (Harrison and Zeitler, 2005). However, He is lost from a crystal through volume diffusion, a process controlled largely by temperature.

In (U-Th)/He thermochronology, minerals eventually cool to a closure temperature at which they no longer lose ^{4}He (Harrison and Zeitler, 2005). The closure temperature is not a specific value because minerals can partially retain He at different rates across a temperature range known as the partial retention zone (PRZ). In the AHe method, the PRZ exists between ~30-90 °C

(Fig. 3) (Flowers et al., 2009). The AHe method has become extremely useful in a variety of geologic studies because of its low closure temperature. AHe's PRZ correlates to ~1-3 km in depth, making AHe useful for studies involving upper crustal processes (Reiners, 2005).

The effective uranium concentration (eU; [U] + 0.235 [Th]) of apatite is a useful measurement for constraining the thermal history of a particular sample. It expresses the α productivity of the decay of both U and Th concentrations. An apatite with higher eU will experience more damage from decay, and the resulting damage traps will impede the ejection of He. This results in a higher closure temperature and higher apparent age for the mineral. Thus, a positive correlation between AHe age and eU indicates relatively slow cooling through the AHe PRZ, while uniform AHe ages across a range of eU values indicates relatively rapid cooling through this temperature window (Flowers et al., 2009). These characteristics make AHe a powerful method for deciphering recent or near-surface phenomena.

3.2 Zircon (U-Th)/He Thermochronology

ZHe is very similar to AHe, by using the (U-Th)/He dating system. However, ZHe has a PRZ as high as 250 °C, depending on cooling rate and grain size (Reiners, 2005) (Fig. 3). Recent studies suggest a lower limit of the PRZ as low as 0 °C (Johnson et al., 2017). This corresponds to depths of 0-6.5 km, assuming a geothermal gradient of 25 °C/km (Reiners, 2005). Like apatite, closure temperatures in zircon are affected by eU, but have a more complex relationship. At lower radiation damage (less than 1.5×10^{18} α/g), He diffusivity rapidly decreases, possibly due to the increasing irregularity of diffusion pathways in the crystal (Guenthner et al., 2013). This results in a positive relationship between ZHe ages and eU, similar to what is observed in the AHe system. However, damage accumulation at α-doses > 1.5×10^{18} α/g becomes so great that damage zones become interconnected and He diffusivity begins to increase, creating an inverse relationship

between ZHe ages and eU (Guenthner et al., 2013). These relationships can be used to differentiate between rapid and slow cooling through the AHe and ZHe PRZs.

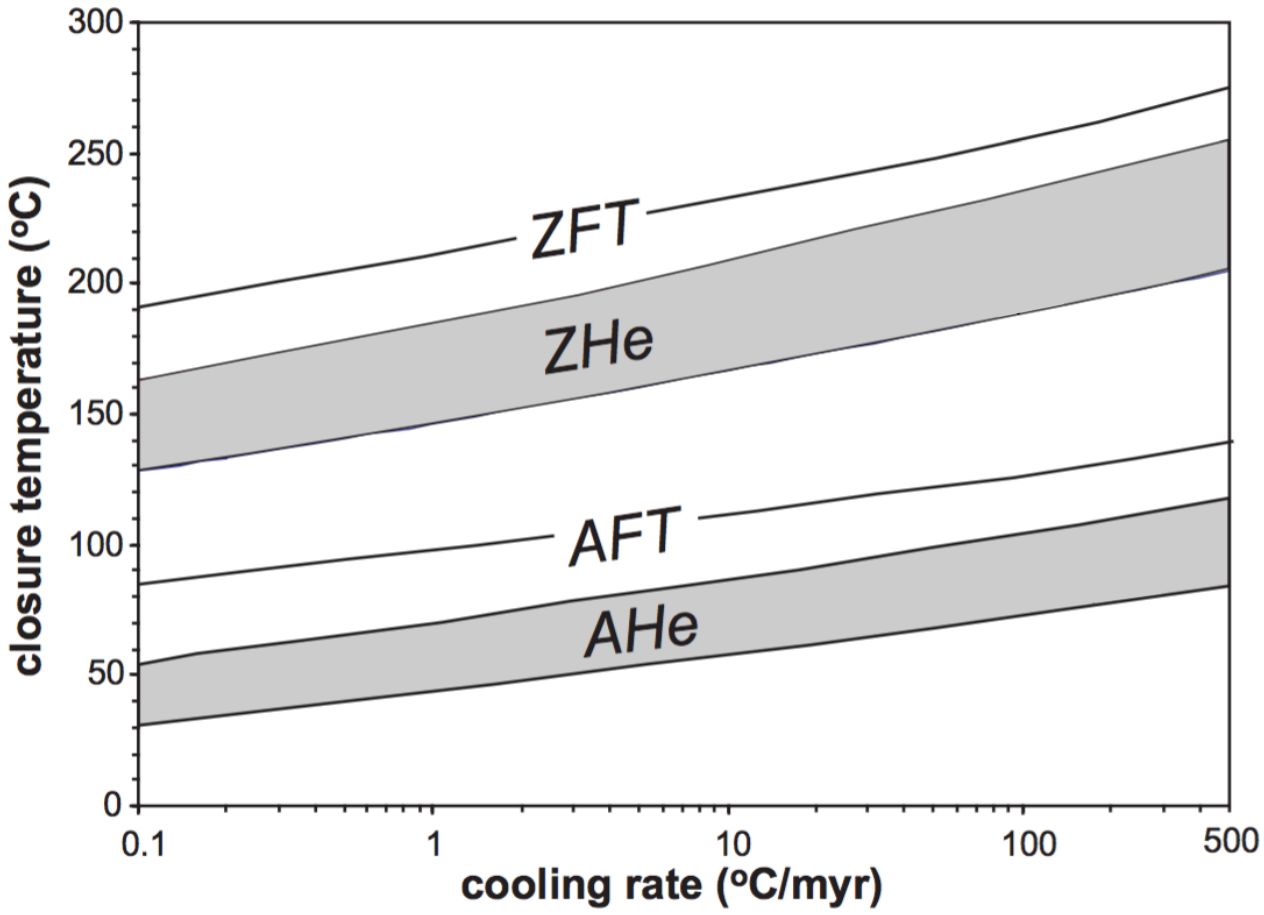

Figure 3: Temperature sensitivity ranges for thermochronologic methods. AFT = apatite fission track; AHe = apatite (U-Th)/He; ZFT = zircon fission track; ZHe = zircon (U-Th)/He. Figure is from Reiners (2005).

3.3 Effects of Lithology and Grain Geometry on Thermochronology

Rock type can have a profound influence on the thermal history interpretation of apatites and zircons. Grains from an igneous rock will have a shared thermal history because they all crystallized at the same time and experienced the same history. For these samples, variations in AHe and ZHe age have a meaningful relationship to eU. For sedimentary samples, individual apatite and zircon crystals are likely derived from different sources. If the sedimentary sample was buried sufficiently, then all accumulated He will diffuse from the apatite and zircon crystal lattices and they will record the same cooling history. However, if a sedimentary sample is not buried deep enough to reset the thermochronologic system of its grains, then these grains will yield different cooling ages and these differences will not show a systematic trend related to grain eU.

3.4 Sample Preparation

Rock samples underwent a process of mineral disaggregation and separation to isolate apatites and zircons. First, the rocks were broken apart using a Braun Chipmunk Jaw Crusher and Bico UA Pulverizer. Next, the crushed samples were sieved to collect material > 710 μm, and then panned in water to sort out fine material. Heavy magnetic minerals were sorted out using a Frantz Magnetic Separator. Finally, zircons and apatites were divided by heavy liquid separation.

Individual grains were handpicked under a microscope. For granitic samples, a total of five apatite crystals and three zircon crystals were selected for dating when possible. For sedimentary samples, ten apatite and six zircon crystals were selected when possible. The crystals were checked to make sure they did not have any visible inclusions, and were selected to be euhedral with a minimum width of 70 μm to reduce error in age calculations. Ages were corrected with the alpha ejection correction F_T, the measure of the amount of He expelled from a crystal (Ketcham et al., 2011). F_T is a geometric correction that assumes a euhedral crystal shape. (U-Th)/He analyses were

performed by the University of Colorado Thermochronology Research and Instrumentation Lab (CU TRaIL), who also performed the age calculations after the methods of Ketcham et al. (2011).

3.5 THERMAL HISTORY MODELING

Due to the complexities involved with AHe/ZHe age and eU values as discussed above, individual ages typically do not date a specific event. Therefore, forward and inverse modeling of ZHe and AHe data was completed using HeFTy software (Ketchum, 2005) in order to constrain each sample's cooling through time. These thermal history models are the primary means of constraining when faults in different regions of the southern Rio Grande rift – Basin and Range transition were active, and for comparing to thermal history models produced for the central and northern segments of the Rio Grande rift (Ricketts et al., 2016).

Inverse modeling with HeFTy uses a Monte Carlo method to plot possible time-temperature paths. The user inputs data about individual grains for a given sample, including measured ZHe or AHe age, grain radius, and concentrations of U, Th, and Sm. HeFTy also allows the user to add in geologic constraints, such as the age of deposition of the sampled rock or known periods of exhumation. Constraints are visualized in HeFTy as rectangles in time-temperature space reflecting the uncertainty of ages and temperatures; paths generated by HeFTy are forced to pass through these constraints (Ketcham, 2005). After all the sample information is entered, HeFTy generates a large amount (specified by the user) of random time-temperature paths. For each path, the program calculates a goodness-of-fit statistic that is predicted to follow a Chi-square probability distribution. HeFTy then saves paths that it calculates to be statistically significant, and categorizes them as "acceptable" or "good" paths (Vermeesch and Tian, 2014).

HeFTy models with ZHe and AHe data in this study begin at the ages of formation of the rocks sampled. Granitic samples with ZHe ages were initially deep enough that they experienced

temperatures above the zircon PRZ (~250 ºC), which would have reset their thermochronologic ages. Therefore, ZHe models were started at a temperature range of 380-400 ºC. Precambrian samples were collected near the Great Unconformity, so models for these samples are forced to surface temperatures of 15 ± 5 ºC at the age of the younger, unconformable Paleozoic rock. Precambrian rocks were assumed to have been buried again and then re-exhumed during later extensional processes. All models end with the samples being at surface temperatures of 15 ± 5 ºC at the Present. The full thermal history of a sample from Precambrian to the Present is important because the samples may have ZHe ages older than known ages of Cenozoic extension. This implies that the samples are recording older cooling events because they were not buried sufficiently deep enough to reset their thermochronologic ages before being cooled by exhumation in the Cenozoic. Thus, zircons can often "remember" their earlier thermal histories.

Samples with only AHe ages use different constraints, regardless of the age of the rock. Because the AHe PRZ has such a low maximum temperature (~90 ºC), it is assumed that the rock was buried deep enough in the past to have reset the AHe system in the crystals. These HeFTy models were started at 90-100 Ma and 190-200 ºC.

All models were run by generating 5000 random time-temperature paths in HeFTy unless otherwise stated. Radiation damage accumulation and annealing models (RDAAM) from Guenthner et al. (2013) and Flowers et al. (2009) were used by HeFTy for zircons and apatites, respectively. Both AHe and ZHe ages were given an uncertainty of 20% of their age to allow for HeFTy to have more variability when choosing time-temperature paths.

Chapter 4: (U-Th)/He Results

4.1 Chiricahua Mountains

The Chiricahua Mountains are a southwest-tilted block in southeast Arizona bounded in the east by the Chiricahua fault (Fig. 2). This buried normal fault separates the Chiricahua Mountains from the downthrown San Simon Valley block. In the late Cretaceous, the range was folded and faulted by Laramide compression (du Bray et al., 1997). Major igneous activity occurred in the Chiricahua Mountains from 29-23 Ma, with volcanic material from the 29 Ma Turkey Creek caldera dominating the central part of the range. Normal faulting coeval with Cenozoic volcanism and plutonism is responsible for the modern topography and position of the Chiricahua Mountains block (Drewes et al., 1995).

Six ZHe and seven AHe ages from two samples were obtained from the middle Proterozoic granodiorite in the northeastern Chiricahua Mountains. The six ZHe ages from both samples together have a mean of 26.87 Ma and all fall within one standard deviation (2.62) of the mean (Table 1). Their eU values ranges from 120 to 265 ppm. AHe ages are generally younger than the ZHe ages, altogether averaging 17.3 Ma (Table 2). eU values range from 40 to 183 ppm. Neither the ZHe nor AHe ages have strong positive correlations with eU (Fig. 4A).

4.2 Peloncillo Mountains

The Peloncillo Mountains in southwestern New Mexico are part of the Basin and Range province, and were uplifted and deformed in the mid to late Tertiary. The Peloncillo Mountains contain a record of Laramide-age igneous activity but no thrust faulting (Gillerman, 1958). Late Cretaceous to early Tertiary andesitic volcanism is also present in the range. Normal faults bound the mountains to the west and east, in the San Simon and Animas Valleys, respectively. The central

Table 1: Zircon (U-Th)/He Data

	Dim. Mass (mg)	Spherical Radius (mm)	4He (nmol/g)	U (ppm)	Th (ppm)	Sm (ppm)	eU	Raw Date (Ma)	Ft	Corrected Date (Ma)	1σ Error (Ma)
Chiricahua Mountains											
16CH01: Precambrian granodiorite, 31.9855°N 107.2477°W, Elev. 1834 m											
z1	5.69	49.11	19.172	170.18	79.95	0.92	189.0	18.79	0.769	24.42	2.31
z2	7.27	55.03	14.883	101.89	77.44	0.50	120.1	22.93	0.791	28.97	2.41
z3	2.89	40.26	24.979	185.28	337.25	1.04	264.5	17.46	0.712	24.48	4.23
									Mean ± st. dev.:	***25.96 ± 2.61 Ma***	
16CH02: Precambrian granodiorite, 31.9908°N 109.2484°W, Elev. 1614 m											
z1	3.25	41.46	21.621	163.14	265.37	1.33	225.5	17.73	0.721	24.55	4.14
z2	4.61	50.46	15.363	102.24	96.11	0.44	124.8	22.77	0.772	29.46	2.67
z3	3.45	43.13	19.771	130.72	165.42	0.59	169.6	21.56	0.734	29.36	4.49
										27.79 ± 2.81 Ma	
Peloncillo Mountains											
16PE01: 33.2 ± 0.2 Ma granite (McLemore et al., 1995), 32.0891°N 108.9734°W, Elev. 1358 m											
z1	4.70	47.60	133.893	1098.29	587.73	2.81	1236.4	20.05	0.762	26.30	3.30
z2	1.59	38.41	129.948	1214.82	709.17	5.08	1381.5	17.42	0.710	24.52	2.85
z3	5.05	52.44	112.370	939.42	504.69	0.83	1058.0	19.67	0.783	25.10	2.03
										25.31 ± 0.90 Ma	
Little Hatchet Mountains											
17LH01: Precambrian granite, 31.7449°N 108.4351°W, Elev. 1646 m											
z1*	3.56	48.27	105.514	147.07	86.37	1.49	167.4	115.76	0.765	150.84	13.43
z2	9.32	61.05	28.319	192.07	97.37	9.67	215.0	24.38	0.812	29.99	2.12
z3	3.42	46.47	48.847	367.23	204.94	1.62	415.4	21.77	0.756	28.75	3.15
										29.37 ± 0.88 Ma	
17LH02: Precambrian granite, 31.7443°N 108.4275°W, Elev. 1438 m											
z1	11.23	65.55	27.820	223.21	108.84	1.72	248.8	20.71	0.825	25.09	1.94
z2	5.38	50.78	19.299	198.41	84.47	11.04	218.3	16.37	0.777	21.06	2.12
z3	3.28	46.19	46.227	321.99	185.53	1.74	365.6	23.40	0.755	30.97	3.31
										25.71 ± 4.98 Ma	
17LH03: Cretaceous sandstone, 31.7824°N 108.4435°W, Elev. 1565 m											
z1	12.15	65.06	48.745	317.63	144.55	0.24	351.6	25.66	0.824	31.14	2.19
z2	5.20	52.36	94.974	696.69	158.91	0.39	734.0	23.96	0.785	30.51	2.63
z3	2.45	38.45	30.445	274.75	113.90	0.57	301.5	18.70	0.709	26.33	4.26
Asterisked grains indicate samples with anomalously high ages not included in the mean.										***29.33 ± 2.61 Ma***	

Cookes Range											
16CR01: Permian sandstone, 32.4466°N 107.6906°W, Elev. 1495 m											
z1	6.64	50.53	48.365	189.33	107.81	0.39	214.7	41.64	0.775	53.68	6.05
z2	3.30	45.70	66.207	159.46	94.36	1.84	181.6	67.21	0.752	89.17	8.29
z3	2.24	39.24	37.628	61.26	57.81	0.47	74.8	92.48	0.711	129.54	22.64
z4	4.87	47.27	24.231	48.16	33.34	0.00	56.0	79.70	0.759	104.75	12.86
z5	2.98	41.26	94.117	176.74	87.31	5.60	197.3	87.81	0.728	120.28	18.92
z6	4.01	50.60	64.176	319.62	132.08	0.03	350.7	33.86	0.776	43.56	3.70
											90.16 ± 35.14 Ma
16CR02: Precambrian granite, 32.3919°N 107.7148°W, Elev. 1435 m											
z1	1.81	39.11	297.308	286.10	86.97	1.97	306.5	177.14	0.716	245.67	33.02
z2	2.04	39.05	222.478	280.75	81.09	14.88	299.8	135.99	0.716	189.00	31.09
z3	2.33	41.04	164.542	255.46	85.36	4.53	275.5	109.73	0.728	150.08	21.59
											194.91 ± 48.07 Ma
Florida Mountains											
16FL05: Cambrian granite, 32.0556°N 107.6722°W, Elev. 2118 m											
z1	3.24	46.06	61.669	439.43	415.49	4.79	537.1	21.24	0.752	28.23	3.08
z2	3.97	48.32	56.230	438.54	494.11	3.68	554.7	18.76	0.761	24.61	2.24
z3	4.96	49.25	69.661	589.83	626.32	3.68	737.0	17.49	0.766	22.81	2.47
											25.22 ± 2.76 Ma
East Potrillo Mountains											
16EP01: Cretaceous sandstone, 31.8860°N 107.0170°W, Elev. 1526 m											
z1	3.28	42.44	25.057	123.20	51.98	1.59	135.4	34.22	0.736	46.45	7.46
z2	2.33	43.03	19.533	195.12	164.75	0.00	233.8	15.47	0.737	20.98	2.12
z3	2.01	39.92	31.198	130.50	64.98	9.17	145.8	39.54	0.720	54.83	7.66
											40.76 ± 17.63 Ma
Franklin Mountains											
17FR02: Cambrian quartzite, 31.8006°N 106.4747°W, Elev. 1381 m											
z1*	4.45	48.66	247.584	122.55	87.25	7.79	143.1	312.33	0.765	404.65	38.43
z2	5.28	51.23	97.848	302.70	304.02	14.85	374.1	48.26	0.775	62.18	5.70
z3*	3.21	44.31	249.788	77.07	57.80	0.00	90.7	489.80	0.744	648.99	89.06
17FR03: Precambrian granite, 31.8397°N 106.4859°W, Elev. 1434 m											
z1	5.33	51.94	173.588	600.98	166.22	1.43	640.0	50.11	0.783	63.93	5.74
z2*	2.97	40.75	186.550	292.32	228.43	1.21	346.0	99.13	0.721	137.03	8.94
z3	3.03	43.00	11.644	132.93	82.70	1.04	152.4	14.16	0.737	19.19	2.46
Asterisked grains indicate samples with anomalously high ages not included in the mean.											***41.56 ± 31.64 Ma***

17FR04: Precambrian granite, 31.8931°N 106.4758°W, Elev. 1477 m											
z1	1.95	34.78	92.779	138.8	79.948	7.0064	157.54	108.18	0.68	158.51	31.43
z2	4.66	50.03	123.690	94.4	75.031	3.5539	112.03	201.21	0.77	259.55	24.29
z3	5.55	50.92	46.577	81.1	57.195	0.0210	94.58	90.62	0.78	116.57	11.60
											178.21 ± 73.49 Ma
Asterisked grains indicate samples with anomalously high ages not included in the mean.											

Table 2: Apatite (U-Th)/He Data

	Dim. Mass (mg)	Spherical Radius (mm)	4He (nmol/g)	U (ppm)	Th (ppm)	Sm (ppm)	eU	Raw Date (Ma)	Ft	Corrected Date (Ma)	1σ Error (Ma)
Chiricahua Mountains											
16CH01: Precambrian granodiorite, 31.9855°N 107.2477°W, Elev. 1834 m											
a1	2.13	46.09	10.547	85.14	205.65	78.98	133.5	14.53	0.682	21.25	1.83
a2	1.36	37.21	5.959	82.47	84.97	77.95	102.4	10.70	0.618	17.25	2.63
a3	2.81	53.11	14.675	132.06	214.59	65.26	182.5	14.83	0.728	20.34	1.44
									Mean ± st. dev.:	***19.61 ± 2.10 Ma***	
16CH02: Precambrian granodiorite, 31.9908°N 109.2484°W, Elev. 1614 m											
a1	3.16	54.00	8.046	106.90	82.86	64.31	126.4	11.74	0.737	15.91	1.21
a2	2.47	45.68	4.597	63.79	39.10	49.45	73.0	11.61	0.694	16.69	1.33
a4	2.33	43.82	2.169	33.01	33.19	34.78	40.8	9.77	0.676	14.41	1.64
a5	2.85	52.98	6.166	84.93	71.57	56.66	101.7	11.17	0.732	15.23	1.10
										15.56 ± 0.97 Ma	
Peloncillo Mountains											
16PE01: 33.2 ± 0.2 Ma granite (McLemore et al., 1995), 32.0891°N 108.9734°W, Elev. 1358 m											
a1	1.64	37.77	2.535	6.57	39.60	59.12	15.9	28.54	0.606	46.36	6.87
a2	1.85	39.84	1.834	9.85	44.73	49.00	20.4	16.29	0.630	25.62	3.31
a3*	2.23	43.58	530.850	14.25	38.91	45.16	23.4	3112.95	0.668	4011.63	463.52
										35.99 ± 14.67 Ma	
Little Hatchet Mountains											
17LH01: Precambrian granite, 31.7449°N 108.4351°W, Elev. 1646 m											
a1	1.91	41.79	2.086	12.10	56.71	68.23	25.4	14.81	0.640	22.92	2.81
Cookes Range											
16CR01: Permian sandstone, 32.4466°N 107.6906°W, Elev. 1495 m											
a6*	3.11	52.22	17.029	2.53	1.19	0.00	2.8	1021.54	0.733	1347.53	105.97
a9*	2.44	46.42	22.117	6.80	4.01	0.00	7.7	506.58	0.699	710.60	51.57
16CR02: Precambrian granite, 32.3919°N 107.7148°W, Elev. 1435 m											
a2	2.20	42.72	0.854	24.39	14.85	41.73	27.9	5.61	0.677	8.25	0.62
a3*	2.19	43.57	6.878	14.00	28.03	46.09	20.6	60.46	0.672	89.21	8.85
a4	7.48	63.87	1.578	37.28	16.35	32.36	41.1	7.07	0.780	9.05	0.66
a5	3.34	47.69	1.824	15.72	33.11	39.55	23.5	14.15	0.697	20.19	1.40
Asterisked grains indicate samples with anomalously high ages not included in the mean.										***12.49 ± 6.68 Ma***	

Florida Mountains											
16FL04: Cambrian granite, 32.0595°N 107.6588°W, Elev. 1770											
a1	2.55	43.10	1.156	10.70	52.85	14.35	23.1	9.18	0.655	13.99	1.43
a2	1.76	39.08	1.122	9.99	61.26	28.94	24.4	8.40	0.619	13.51	1.83
a3	1.67	33.53	1.703	16.93	79.74	23.68	35.7	8.77	0.558	15.64	2.82
a4	1.77	39.43	1.190	14.84	57.05	23.44	28.3	7.73	0.630	12.22	1.43
a5	3.34	50.49	0.201	2.31	12.72	2.40	5.3	6.96	0.704	9.87	0.78
											13.05 ± 2.15 Ma
16FL05: Cambrian granite, 32.0556°N 107.6722°W, Elev. 2118 m											
a3	1.94	46.25	0.579	2.39	19.81	17.59	7.0	14.85	0.670	22.00	1.70
Asterisked grains indicate samples with anomalously high ages not included in the mean.											

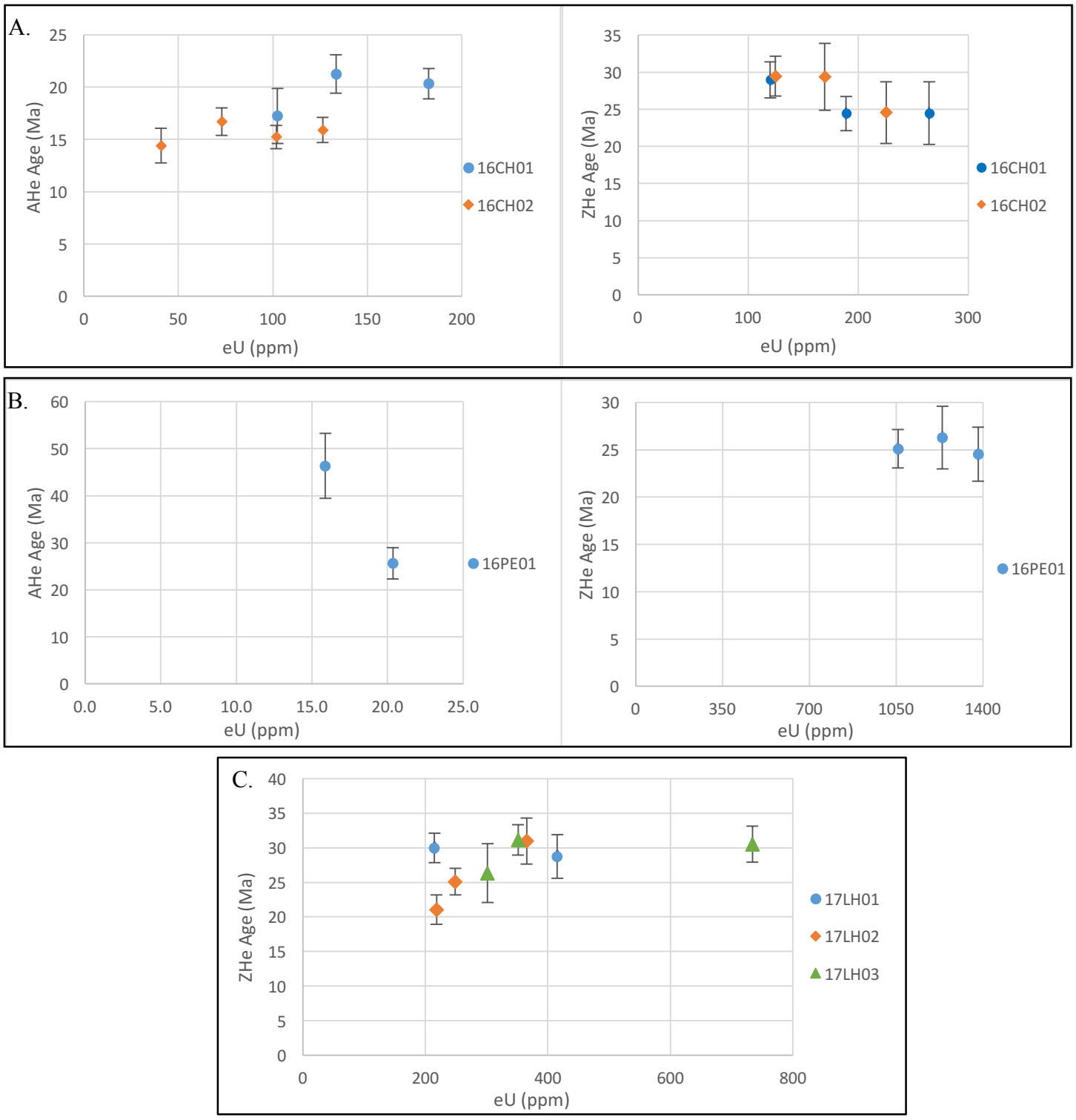

Figure 4: Age vs. eU plots for the A. Chiricahua Mountains, B. Peloncillo Mountains, and C. Little Hatchet Mountains.

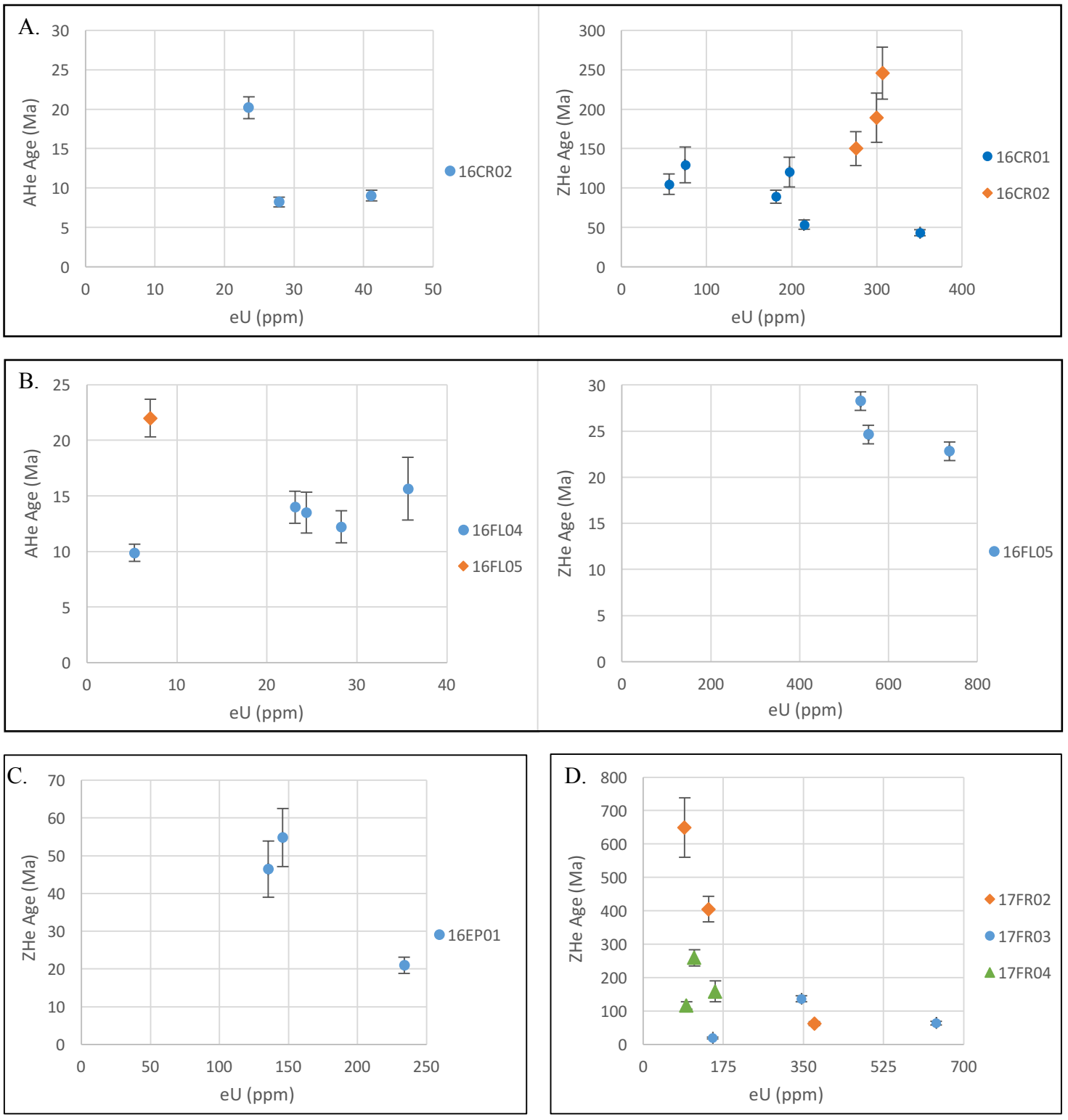

Figure 5: Age vs. eU plots for the A. Cookes Range, B. Florida Mountains, C. East Potrillo Mountains, and D. Franklin Mountains.

part of the range consists primarily of southwest tilted fault blocks. The central range includes the Granite Gap, part of an east-west trending upthrown block, bounded by south-dipping normal faults. The relation between the Granite Gap faults and the other faults in the range is unclear, but the Granite Gap faults appear to offset the north-trending Basin and Range blocks.

Three ZHe and three AHe ages from one sample were collected from the 33.2 Ma (McLemore et al., 1995) Granite Gap granite in the central Peloncillo Mountains. The ZHe ages have a mean of 25.31 Ma and high eU (between 1058 and 1380 ppm) (Table 1). Two of the apatite crystals from the Peloncillo Mountains yield AHe ages < 50 Ma and eU concentrations < 21 ppm (Table 2). An anomalously large AHe age (4011 Ma) was recorded in one crystal, and most likely represents an undetected inclusion in the crystal. The grain was removed from further consideration in this study. ZHe and eU show no strong positive or negative correlation, while AHe age and eU have a negative correlation (Fig. 4B).

4.3 Little Hatchet Mountains

The geology of the Little Hatchets in southwestern New Mexico is dominated by Laramide thrust faulting and folding that makes up most of the range's structure. Late Cretaceous volcanism associated with the Laramide is present throughout the Little Hatchet Mountains as well. A second pulse of igneous activity in the Eocene resulted in a granitic intrusion in the southern part of the range. The modern topography of the Little Hatchet Mountains is the product of Basin and Range normal faulting. The boundary faults strike northward along the east and west sides of the range (Zeller, 1970).

Six ZHe and one AHe ages from two samples were collected from the Precambrian granite in the southernmost end of the Little Hatchet Mountains. Three ZHe ages from one sample were obtained from the sandstone member of the Cretaceous Mojado formation north of Granite Pass.

Excluding a 150 Ma outlier, the ZHe ages altogether have a mean of 27.98 Ma (Table 1). The zircons have a large spread in eU, between 167 and 734 ppm; the 150 Ma grain has the lowest eU. The one apatite crystal has an AHe age of 22.92 Ma, within the range of the ZHe samples' ages, but the eU (25.4 ppm) is significantly lower (Table 2). Zircons from sample 17LH02 have a positive relationship between ZHe age and eU, while the other two samples show no strong positive or negative relationship (Fig. 4C).

4.4 COOKES RANGE

Situated north of Deming, NM, the Cookes Range is a south-tilted, roughly triangular block bounded by normal faults on three sides. The range experienced igneous activity in the Paleogene, including volcanoclastic flows from the Mogollon-Datil volcanic field to the north (Clemons, 1982). Extension in the region, resulting in the uplifting of the modern Cookes Range block, began in the Cenozoic. The system of normal faults in the range offsets basalts as young as 28 Ma.

Six ZHe and two AHe ages were obtained from sample 16CR01 from the sandstone member of the Permian Abo formation in the Cookes Range. The ZHe ages range from about 40 to 140 Ma and have a large spread in eU from 56 to 350 ppm (Table 1). ZHe and eU in this sample have a weak negative correlation (Fig. 5A). The AHe ages are both anomalously high, likely because of unrecognized inclusions, and were removed from further consideration in this study.

Three ZHe and four AHe ages were obtained from sample 16CR02 from Precambrian granite. The ZHe ages range from about 130 to 280 Ma, and have high eU values from 275 to 307 ppm (Table 1). ZHe and eU in this sample have a positive correlation (Fig. 5A). Excluding an 89 Ma outlier with a relatively high eU, the AHe ages have a mean of 12.49 Ma and an eU range from 5 to 14 ppm (Table 2). AHe and eU have a weak negative correlation (Fig. 5A).

4.5 Florida Mountains

The Florida Mountains are a northeast tilted block south of Deming, NM, bounded by north-trending normal faults situated to the east and west of the range. Laramide deformation in the region created a basement-cored uplift along the south Florida Mountains fault, which cuts rocks as young as the Eocene Lobo Formation (Clemons, 1998). The Florida Mountains block was uplifted and tilted to its present position along the west Florida Mountains fault, which was active beginning in the Miocene and into the Pleistocene.

Three ZHe and six AHe samples were obtained from two samples from Cambrian granite along the west side of South Peak in the Florida Mountains. All three ZHe ages are from one sample, 16FL05. They have a mean of 25.22 Ma and high eU values from 537 to 737 ppm (Table 1). ZHe age and eU have a negative correlation (Fig. 5B). The five AHe ages from sample 16FL04 have a mean of 14.54 Ma, and a small spread in eU from 6.9 to 9.2 ppm. The one AHe age from 16FL05 has a relatively higher age of 22.00 Ma (Table 2). In 16FL04, AHe age and eU have a positive correlation (Fig. 5B).

4.6 East Potrillo Mountains

The East Potrillo Mountains in south-central New Mexico are a horst block bounded by the East Potrillo fault to the northeast and the Mt. Riley fault zone to the southwest. The range contains a system of late Oligocene – early Miocene low angle normal faults that crosscut late Cretaceous – early Tertiary compressional structures (Seager and Mack, 1994). These structures are Laramide thrust sheets and associated drag folds that increase in deformational severity towards the north of the range. Mid-Paleogene extension in the East Potrillos has been estimated to be 75-100%, similar to estimates of extension across the central Rio Grande rift, indicating that the Potrillo Mountains were uplifted during this later period of extensional tectonism.

Three ZHe ages from one sample were obtained from the sandstone member of the Cretaceous U-Bar Formation in the East Potrillo Mountains. They have a mean age of 40.76 Ma and an eU range between 135 and 234 ppm (Table 1). The ZHe age and eU have a negative correlation (Fig. 5C).

4.7 Franklin Mountains

The Franklin Mountains are a north-trending west-tilted block in El Paso, Texas, east of the Mesilla Basin in the Rio Grande rift. The mountains record both thin- and thick-skinned Laramide deformation and represent a transition between the two deformation styles in the Chihuahua trough (Carciumaru and Ortega, 2008). Rio Grande rift associated uplift of the Franklin Mountains is thought to have occurred in the Miocene (Harbour, 1972). Based on fault scarp morphology, the latest movement along the East Franklin boundary fault occurred in the Pleistocene or early Holocene (Machette, 1987).

Three ZHe ages from one sample were obtained from the Cambrian Bliss Formation, and six ZHe ages from two samples were obtained from the Precambrian Red Bluff granite suite. Two grains from the Bliss have anomalously high ZHe ages, but together all three grains have a negative correlation between ZHe age and eU. There is a high spread in eU, between 90 and 375 ppm (Table 1). Sample 17FR03 has a high spread in ZHe age from 19 to 137 Ma, and in eU from 152 to 640 ppm. Sample 17FR04 has anomalously high ZHe ages between 116 and 260 Ma, and a large spread in eU from 90 to 202 ppm. None of the Red Bluff samples have strong positive or negative correlations between ZHe age and eU (Fig. 5D).

Chapter 5: Thermal History Modeling and Interpretation

5.1 Chiricahua Mountains

Both Chiricahua samples, 16CH01 and 16CH02, were run in HeFTy with the same geologic constraints, and used all ZHe and AHe ages available (Table 3). The Precambrian granodiorite does not have a well-constrained age of formation but it is unconformably overlain by the Cambrian-Ordovician Bliss Formation. The granodiorite would have been at the Earth's surface during the Bliss's deposition, so the samples experienced surface temperatures of 15 ± 5 ºC between 480-500 Ma, and the HeFTy models start with these conditions. It was not necessary to begin the models in the Precambrian because the ZHe and AHe ages were not older than the Cenozoic, and thus did not record any cooling before then.

Both thermal history models record cooling initiating before 27 Ma (Fig. 6). 16CH01 shows cooling to near surface temperatures between 30 and 14.8 Ma, while 16CH02 shows cooling between 19.8 and 12.5 Ma. The period of earlier cooling in sample 16CH01 is consistent with its higher elevation, since it would have been exhumed before 16CH02. The cooling range for both samples are consistent with Basin and Range extension in the Desert Southwest region of Arizona, which occurred from less than 30 to 12 Ma (Dickinson, 2002). The close (U-Th)/He ages and large spreads in eU indicate relatively rapid cooling of the rock.

5.2 Peloncillo Mountains

Sample 16PE01 was run in HeFTy starting between 32.9 and 29.8 Ma, the range of K-Ar dates for the granite sample (McLemore et al., 1995). The anomalously high AHe age from this sample was not included in the model (Table 3). The HeFTy model shows cooling to near-surface temperatures between 32.2 and 24.7 Ma (Fig. 7). The close ZHe ages and large spread in eU indicate relatively rapid cooling of the granite; the negative relationship between AHe and eU is

Table 3: Grains used in HeFTy models

Mountain Range	Model	# of ZHe Ages Used	Grains	# of AHe Ages Used	Grains
Chiricahuas	16CH01	3	z1, z2, z3	3	a1, a2, a3
	16CH02	3	z1, z2, z3	4	a1, a2, a4, a5
Peloncillos	16PE01	3	z1, z2, z3	2	a1, a2
Little Hatchets	17LH01	2	z2, z3	1	a1
	17LH02	3	z1, z2, z3	N/A	
	17LH03	3	z1, z2, z3	N/A	
Cookes	16CR01a	3	z1, z2, z6	0	N/A
	16CR01b	4	z2, z3, z4, z5	0	N/A
	16CR02	0	N/A	3	a2, a4, a5
Floridas	16FL04	N/A		5	a1, a2, a3, a4, a5
	16FL05	3	z1, z2, z3	1	a3
E. Potrillos	16EP01a	2	z1, z3	N/A	
	16EP01b	1	z2		
Franklins	17FR02	1	z2	N/A	
	17FR03	2	z1, z3	N/A	
	17FR04	3	z1, z2, z3	N/A	

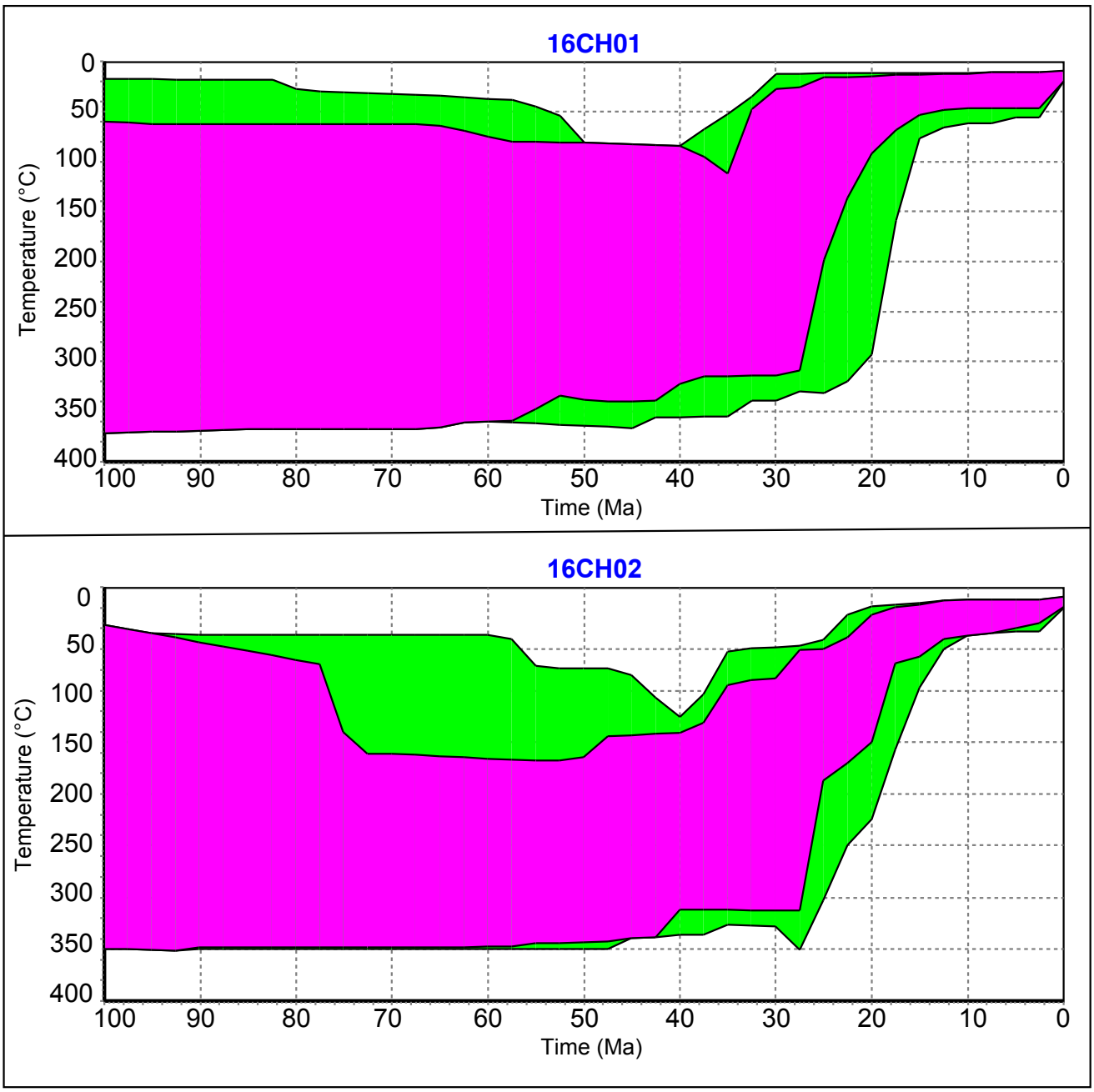

Figure 6: Chiricahua Mountains thermal history models. Green envelopes represent “acceptable” time-temperature paths, and purple envelopes represent “good” paths.

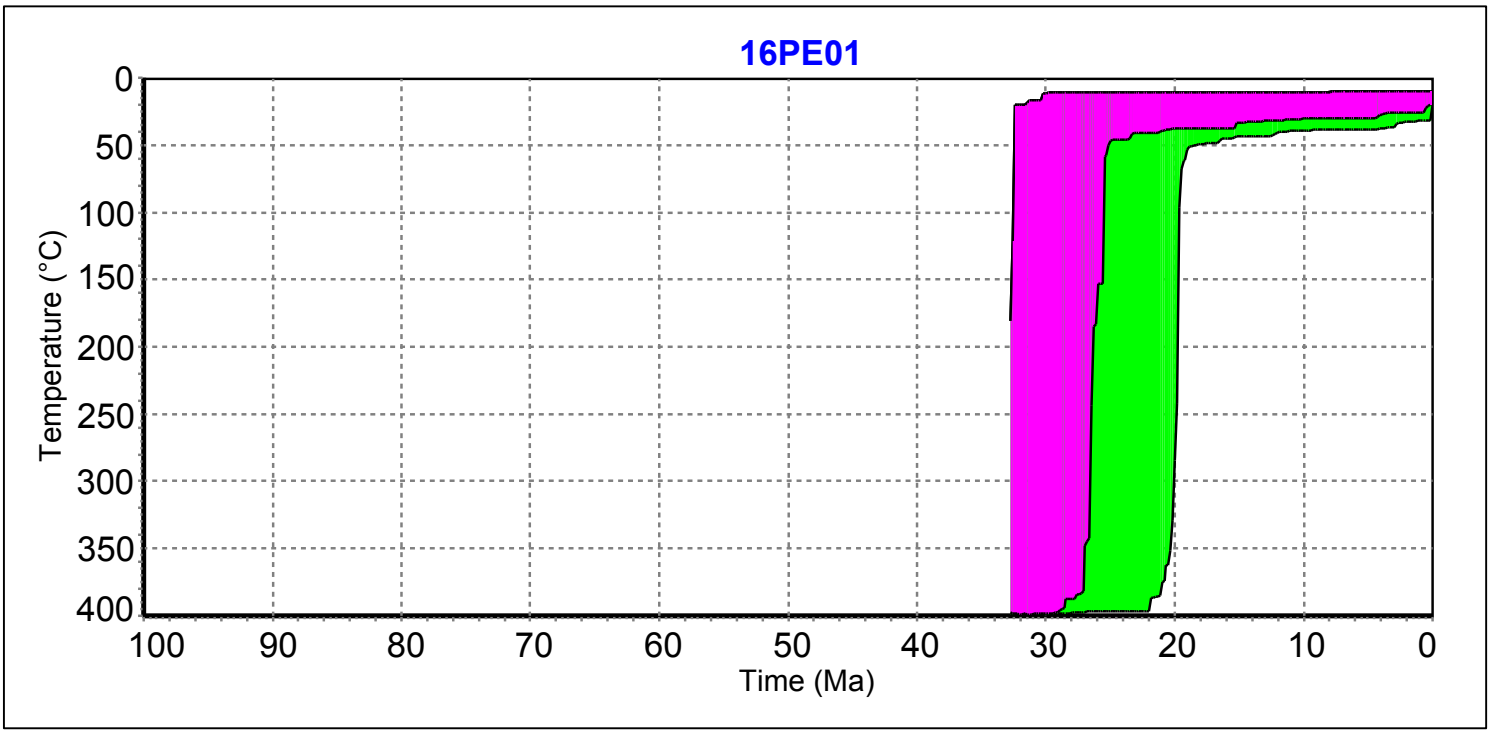

Figure 7: Peloncillo Mountains thermal history model. Green envelopes represent "acceptable" time-temperature paths, and purple envelopes represent "good" paths.

difficult to interpret and gives little information on the cooling history. Because of the rapid cooling close to the age of formation of the rock, the Granite Gap pluton may have been emplaced shallowly in the crust. The thermal history may reflect the cooling of the newly formed rock and may not be strongly controlled by rift-related uplift and exhumation.

5.3 Little Hatchet Mountains

The two samples from the Precambrian granite, 17LH01 and 17LH02, were modeled with the same geologic constraints. The granite has an uncertain absolute age, but rapakivi granites from the same igneous suite have been dated to about 1100 Ma (McLemore et al., 2012), so the age of formation was modeled to be between 1100 and 1000 Ma. The granite is unconformably overlain by the Pennsylvanian-Permian Horquilla limestone, and that was used in HeFTy to enforce another constraint on the thermal history. The rock would have experienced surface temperatures of 15 ± 5 ºC at 323 to 280 Ma.

In model 17LH01, grain z1 wasn't used for the model because of its anomalously high ZHe age of 150.8 Ma (Table 3). This model shows that cooling to near-surface temperatures occurred between 27.2 and 16.2 Ma (Fig. 8). For 17LH02, cooling to the surface was as early as 25.8 Ma, but the minimum cooling age is poorly constrained, partly because of a lack of AHe data for this sample (Fig. 8). Given the similar maximum ages of cooling between the two samples, there may be a similar minimum. The lack of a strong positive or negative correlation between ZHe and eU in 17LH01 and 17LH02 indicates relatively slow cooling of the rock.

Sample 17LH03 from the Albian Mojado formation was modeled to have formed at surface temperatures of 15 ± 5 ºC between 113 and 100 Ma. The HeFTy model recorded cooling as early as 32.2 Ma (Fig. 8). An age of minimum cooling is poorly constrained because of a lack of AHe

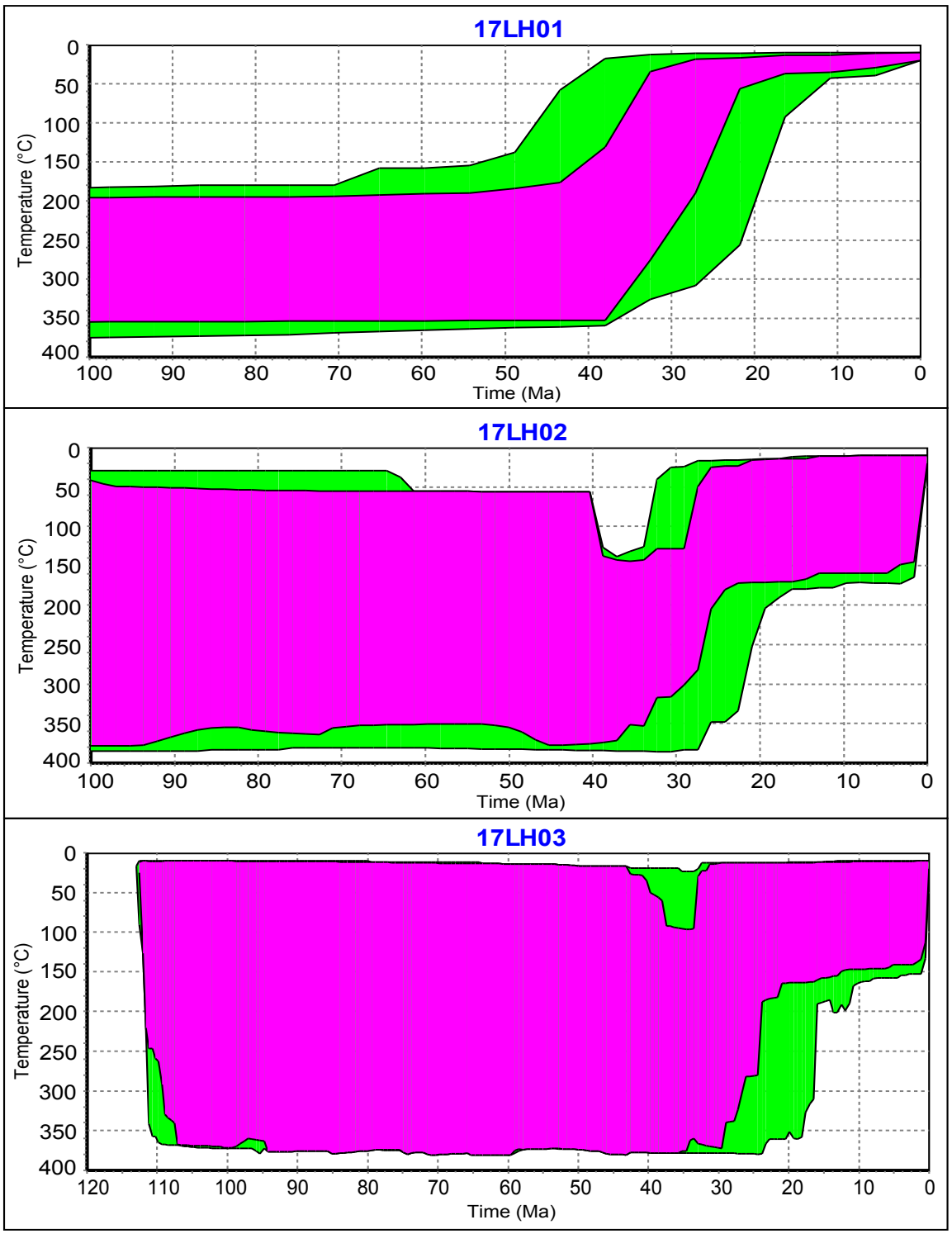

Figure 8: Little Hatchet Mountains thermal history models. Green envelopes represent "acceptable" time-temperature paths, and purple envelopes represent "good" paths.

data for this sample, but it may be close to the 16.2 Ma minimum from 17LH01. The large spread in eU and close ZHe ages indicate slow cooling of the rock. This sample along with the others from the Little Hatchet Mountains have cooling ranges consistent with the age range of Desert Southwest extension.

5.4 COOKES RANGE

Sample 16CR01 from the Permian Abo formation was modeled to have formed at surface temperatures of 15 ± 5 ºC between 300 and 250 Ma. The model omits the two anomalously high AHe ages for this sample, whose ages are assumed to be due to undetected inclusions in the grains. HeFTy would not produce a model with all six zircon grains, so two separate models were run. 16CR01a uses grains z1, z2, and z6, while 16CR01b uses grains z2-z5 (Table 3). 16CR01a records cooling between 60 and 54 Ma (Fig. 9), but 16CR01b does not record any Cenozoic cooling events (Fig. 9). Because most of the ZHe ages are older than periods of extension in the Rio Grande rift and Basin and Range, the crystals may not have been sufficiently buried deep enough after deposition to reset the (U-Th)/He thermochronologic system and record post-Eocene cooling. This is supported by the cross-sections from the Cookes Range, which show < 1 km of rock above the Abo before the Oligocene (Clemons, 1982). Faulting in the Cookes Range was conjectured by Clemons (1982) to be associated with Laramide deformation, so cooling modeled in 16CR01a may represent Laramide uplift. However, this remains speculative because there exists no detailed study of the range's structure, and half the grains in the sample were excluded from the model.

16CR02 used exclusively AHe ages because the sample's ZHe ages were all older than the Cenozoic (Table 3). Apatite grain a3 was also omitted from the model because of its relatively high AHe age. Because the AHe PRZ has such a low maximum temperature (~90 ºC), this model

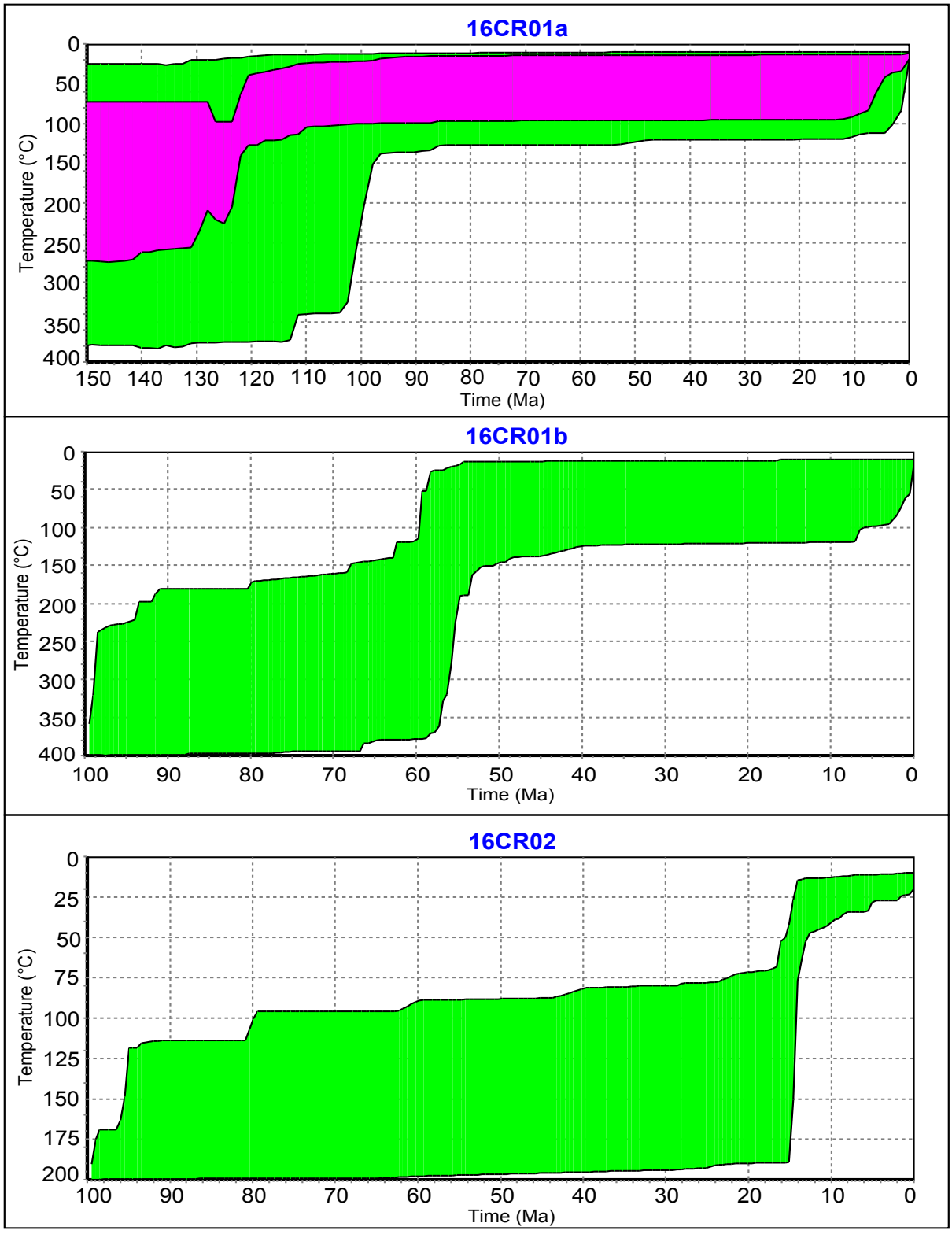

Figure 9: Cookes Range thermal history models. Green envelopes represent "acceptable" time-temperature paths, and purple envelopes represent "good" paths.

assumes that the rock was buried deep enough to have reset the AHe system in the crystals. The model was started at 90-100 Ma and 190-200 ºC. The HeFTy model shows cooling between 16.4 and 12.4 Ma (Fig. 9). The lack of a positive relationship between AHe age and eU indicates that the sample cooled slowly.

5.5 Florida Mountains

16FL04 used exclusively AHe ages (Table 3). Because the AHe PRZ has such a low maximum temperature (~90 ºC), this model assumes that the rock was buried deep enough to have reset the AHe system in the crystals. The model was started at 90-100 Ma and 190-200 ºC. Because 16FL05 has a mix of ZHe and AHe ages, the model needed to be started at a higher temperature and needed to include geologic constraints on the Cambrian granite sample. The granite has an uncertain absolute age, but is unconformably overlain by the Bliss sandstone, so the model was started at 15 ± 5 ºC between 480-500 Ma.

16FL04 recorded cooling to near surface temperatures between 17 and 14 Ma (Fig. 10), while 16FL05 showed cooling between 27.5 and 17.6 Ma (Fig. 10). 16FL05 was taken from a higher elevation than 16FL04 and thus would have cooled earlier, agreeing with the outcomes of the HeFTy models. The ZHe and AHe ages show no strong positive or negative relationship with eU concentration, indicating that the samples cooled slowly.

5.6 East Potrillo Mountains

Sample 16EP01 was run in HeFTy starting between 113 and 100 Ma, the age range of the Albian stage, from which the U-bar formation originates. Since the sample came from a sedimentary rock, it was modeled as having been formed at surface temperatures of 15 ± 5 ºC. Because of the difference between the ZHe ages of the sample, two models were run. The first,

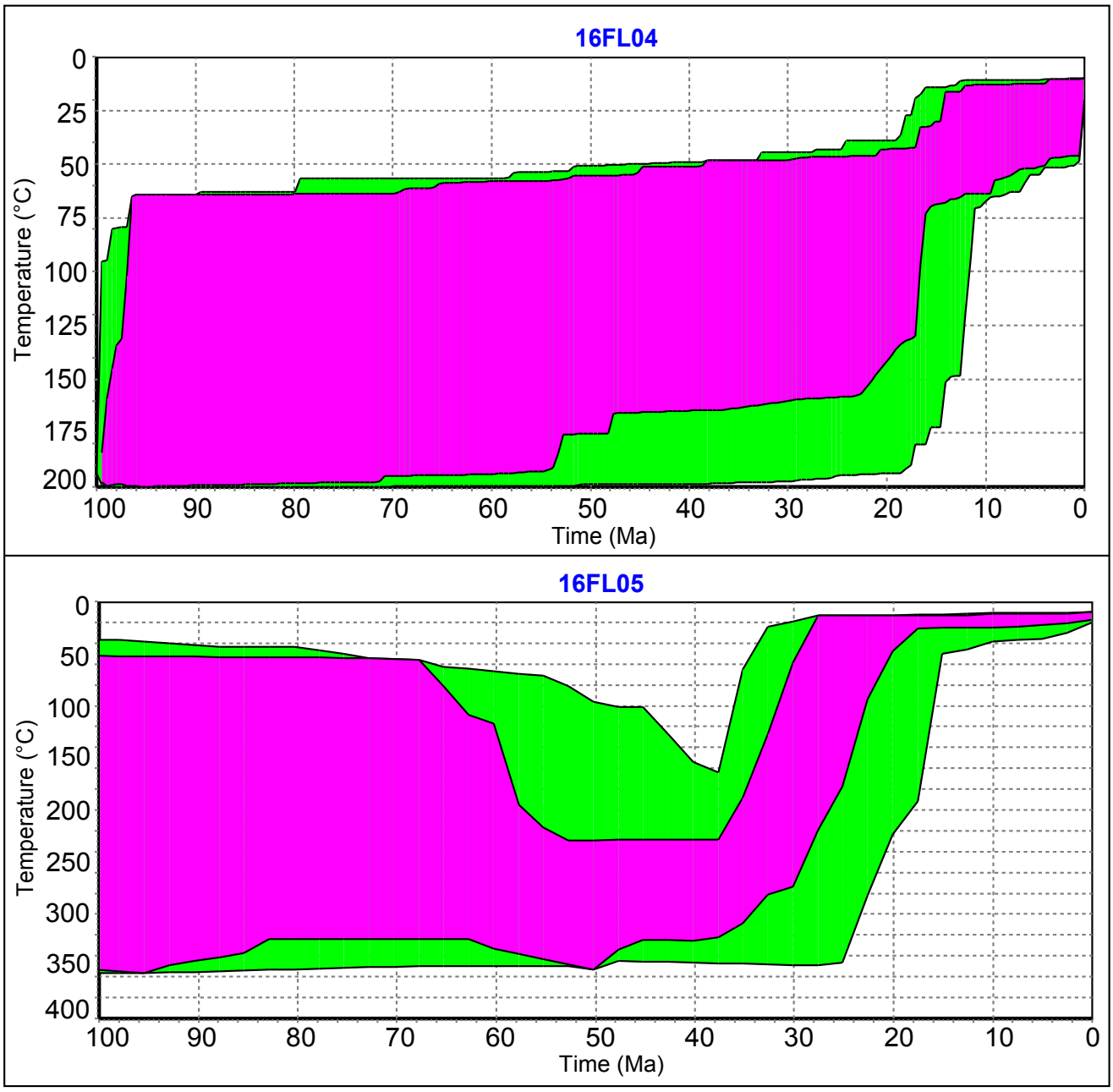

Figure 10: Florida Mountains thermal history models. Green envelopes represent "acceptable" time-temperature paths, and purple envelopes represent "good" paths.

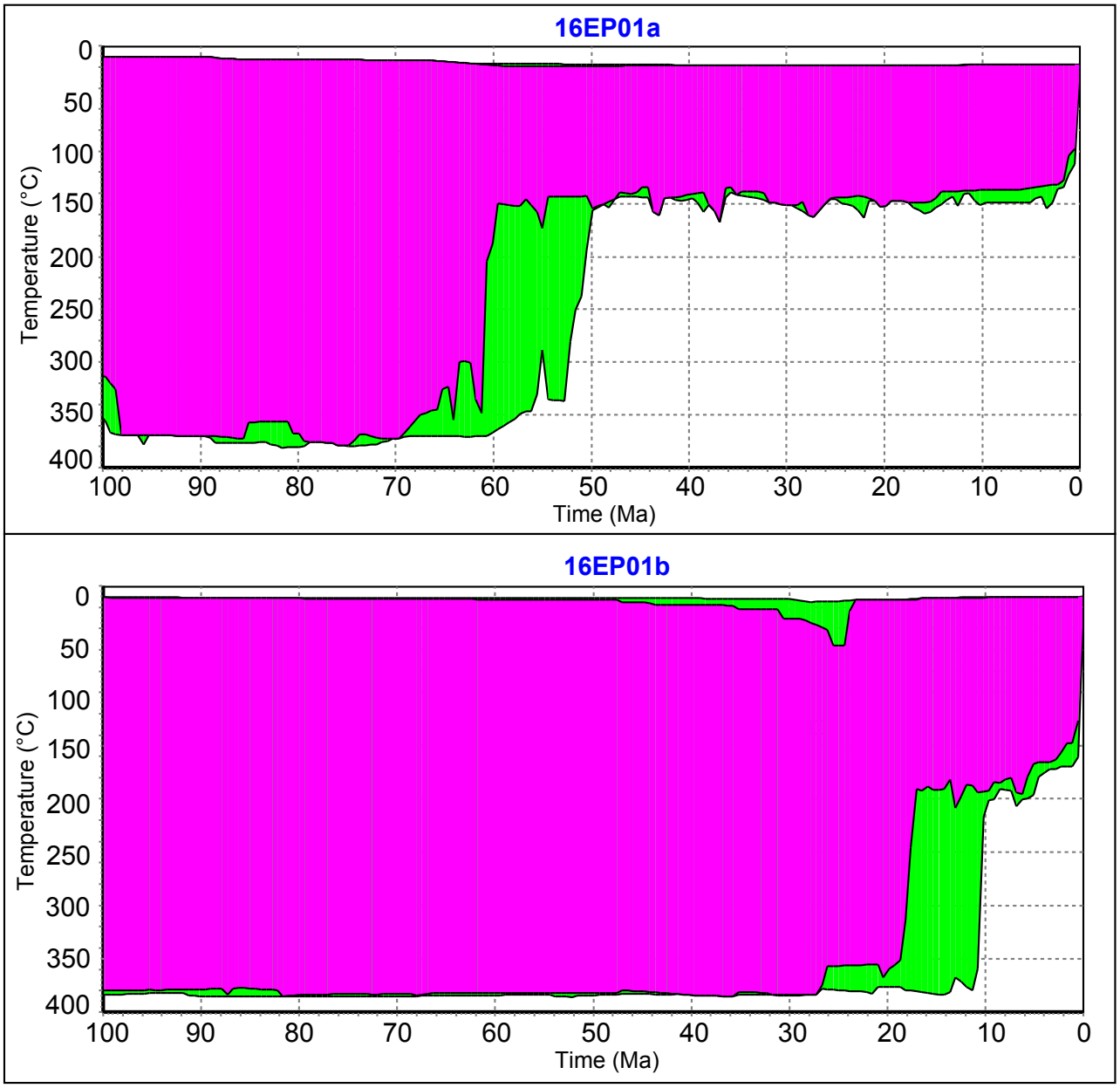

Figure 11: East Potrillo Mountains thermal history models. Green envelopes represent "acceptable" time-temperature paths, and purple envelopes represent "good" paths.

16EP01a, used grains z1 and z3, while the second, 16EP01b, used grain z2 (Table 3). The resulting thermal history models do not show any Cenozoic cooling events (Fig. 11). Because the mean ZHe age predates rifting, the crystals may not have been sufficiently buried deep enough after deposition to reset the (U-Th)/He thermochronologic system. This is further supported by the stratigraphy of the East Potrillos, which records < 700 m of rock above the U-bar by the middle Oligocene (Seager and Mack, 1994), and which is significantly less than the 5.7 km that corresponds to the ZHe PRZ.

5.7 Franklin Mountains

Sample 17FR02 from the Cambrian-Ordovician Bliss Formation was run in HeFTy starting at surface temperatures of 15 ± 5 ºC beginning from 500 to 480 Ma. Grain z3 was not run because of its anomalously high ZHe age, older than the age of the Bliss. Samples 17FR03 and 17FR04 were both from the 1120 Ma (Shannon et al., 1997) Red Bluff suite and so their models were started at 1100-1000 Ma. Because the Red Bluff is unconformably overlain by the Bliss Formation, these models were further constrained to pass through temperatures of 15 ± 5 ºC from 500-480 Ma. In 17FR03, grain z2 was excluded from modeling because of its relatively high ZHe age.

HeFTy did not find any acceptable or good time-temperature paths form 17FR02 using grains z1 and z3, so the model was rerun with only grain z2 (Table 3). The thermal history model shows a cooling event between about 70 and 55 Ma, which may suggest Laramide-age uplift (Fig. 12). However, given that the model was run with only one ZHe age and the other ages were much older, this interpretation is only a speculation.

The thermal history model for 17FR04 do not record any Cenozoic cooling events (Fig. 12). 17FR03 records cooling between 13 and 2.2 Ma (Fig. 12). Given the high ZHe ages,

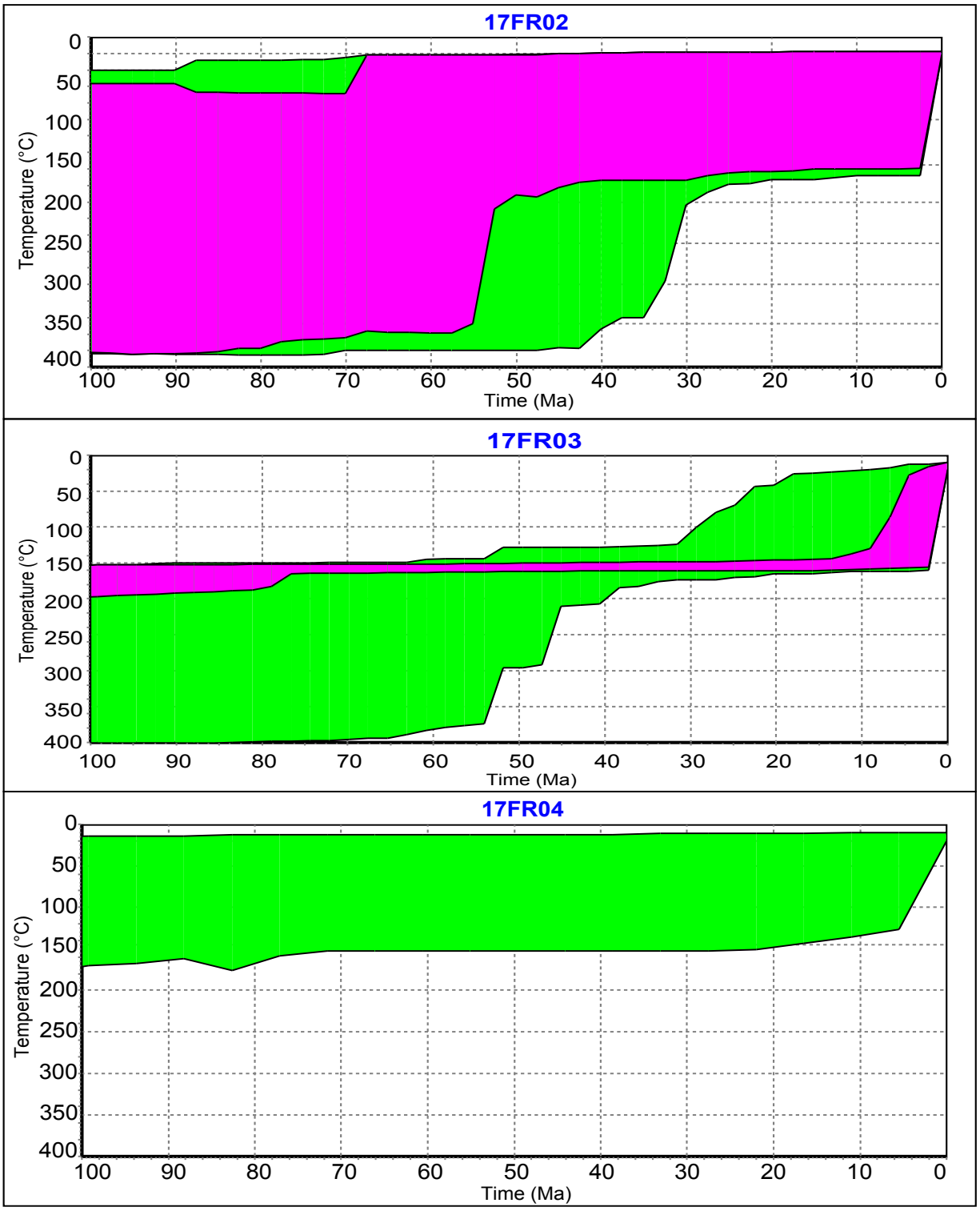

Figure 12: Franklin Mountains thermal history models. Green envelopes represent "acceptable" time-temperature paths, and purple envelopes represent "good" paths.

17FR02 and 17FR04 may not have been buried deep enough to reset the (U-Th)/He thermochronologic system. However, 17FR03 produced a thermal history with Cenozoic cooling despite having experienced similar burial depths. 17FR03 was sampled from an upthrown block along the McKelligon Canyon fault in the Franklins, which may have been active during the mountain-building of the Franklins (Lovejoy, 1975). Therefore, the sample may have been buried deep enough to reset the crystals' thermochronologic system, and its cooling history reflects the rock's uplift along the McKelligon Canyon fault. The large spread in eU and the lack of a strong positive or negative relationship between eU and ZHe age indicate that the sample cooled slowly.

Chapter 6: Discussion

6.1 Boundary between the Basin and Range Province and Rio Grande Rift

Given the differences in heat flow, gravity, and crustal thickness in the Basin and Range and Rio Grande rift in southern New Mexico (e.g., Keller et al., 1990), it is likely that the two are separate tectonic provinces. Plots of eU versus ZHe age for all the mountain ranges in this study, with the data separated by tectonic province (Fig. 13), were created to evaluate the boundaries previously proposed by Woodward et al. (1978) and Mack (2004) (Fig. 2). When the Rio Grande rift includes the Cookes Range and the Florida Mountains, there is a distinct difference between ZHe ages in the rift and the Basin and Range (Fig. 13). Rift samples have a large spread in ZHe ages, with most of the ages much older than the rift itself. Except for a 150 Ma outlier from the Little Hatchet Mountains, Basin and Range samples have ZHe ages between 20 and 32 Ma. This pattern is lost when samples are sorted using the rift boundary to the east of the Cookes and Floridas (Fig. 13). AHe samples were also plotted to compare the two boundaries (Fig. 14). AHe data previously obtained from the Franklin Mountains (Delfin and Ricketts, 2016) and the Organ and San Andres Mountains (Ricketts et al., 2016) were also included. Regardless of the location of the Basin and Range – Rio Grande rift boundary, AHe samples in the Basin and Range tended to have higher eU, and a majority of the ages for all samples were less than 30 Ma.

ZHe ages plotted versus their longitude (Fig. 15) similarly suggest a boundary between the Rio Grande rift and Basin and Range to the west of the Cookes Range. Rift samples have large ZHe ages, especially in the Cookes and Franklins. AHe ages (Delfin and Ricketts, 2016; Ricketts et al., 2016; this study) plotted versus their longitude (Fig. 15) do not show the same pattern. AHe ages are generally less than 25 Ma, except for outliers in the Cookes Range and Peloncillo Mountains. The Franklin Mountains are the only location with a larger range in AHe ages.

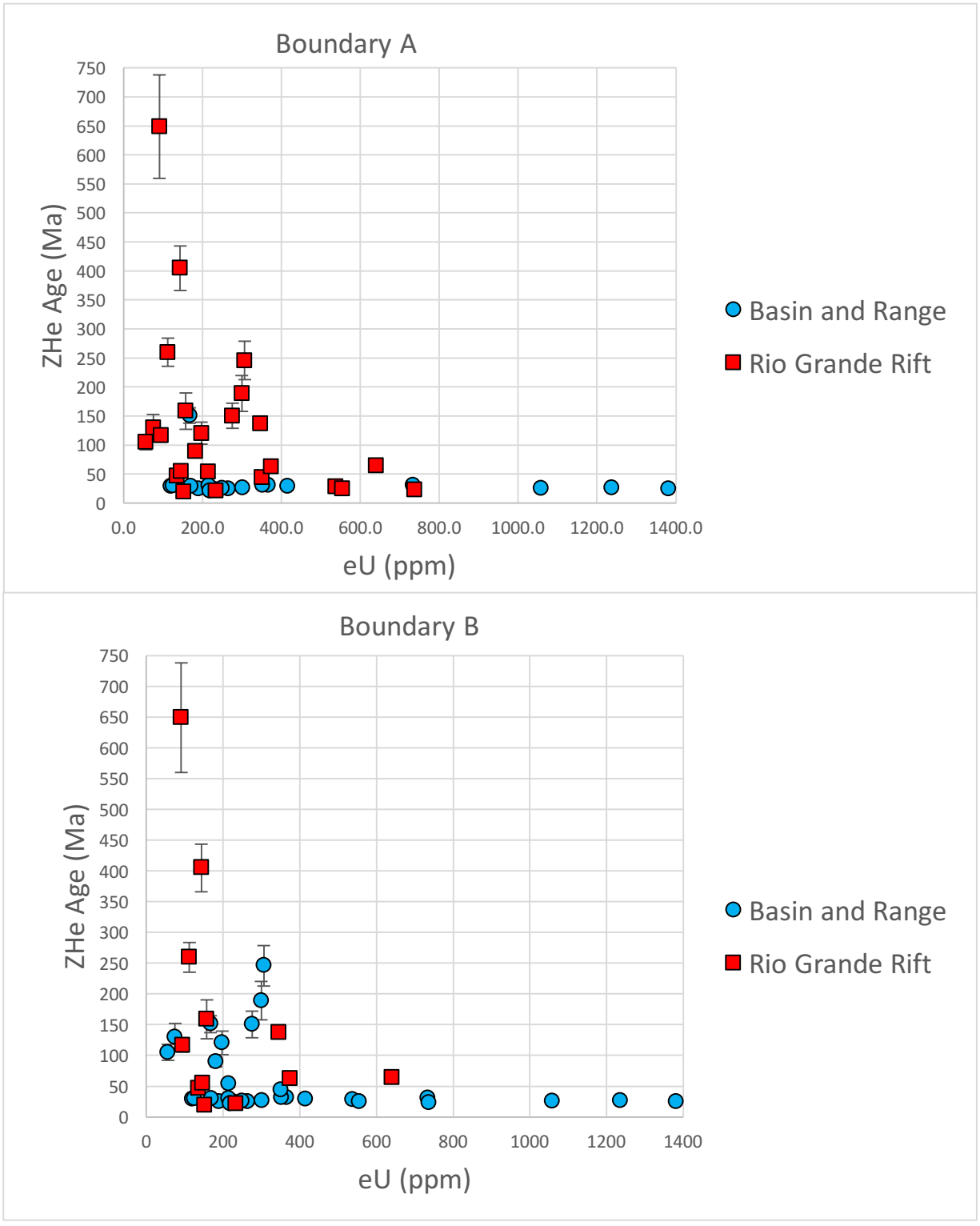

Figure 13: ZHe age vs. eU sorted by tectonic province

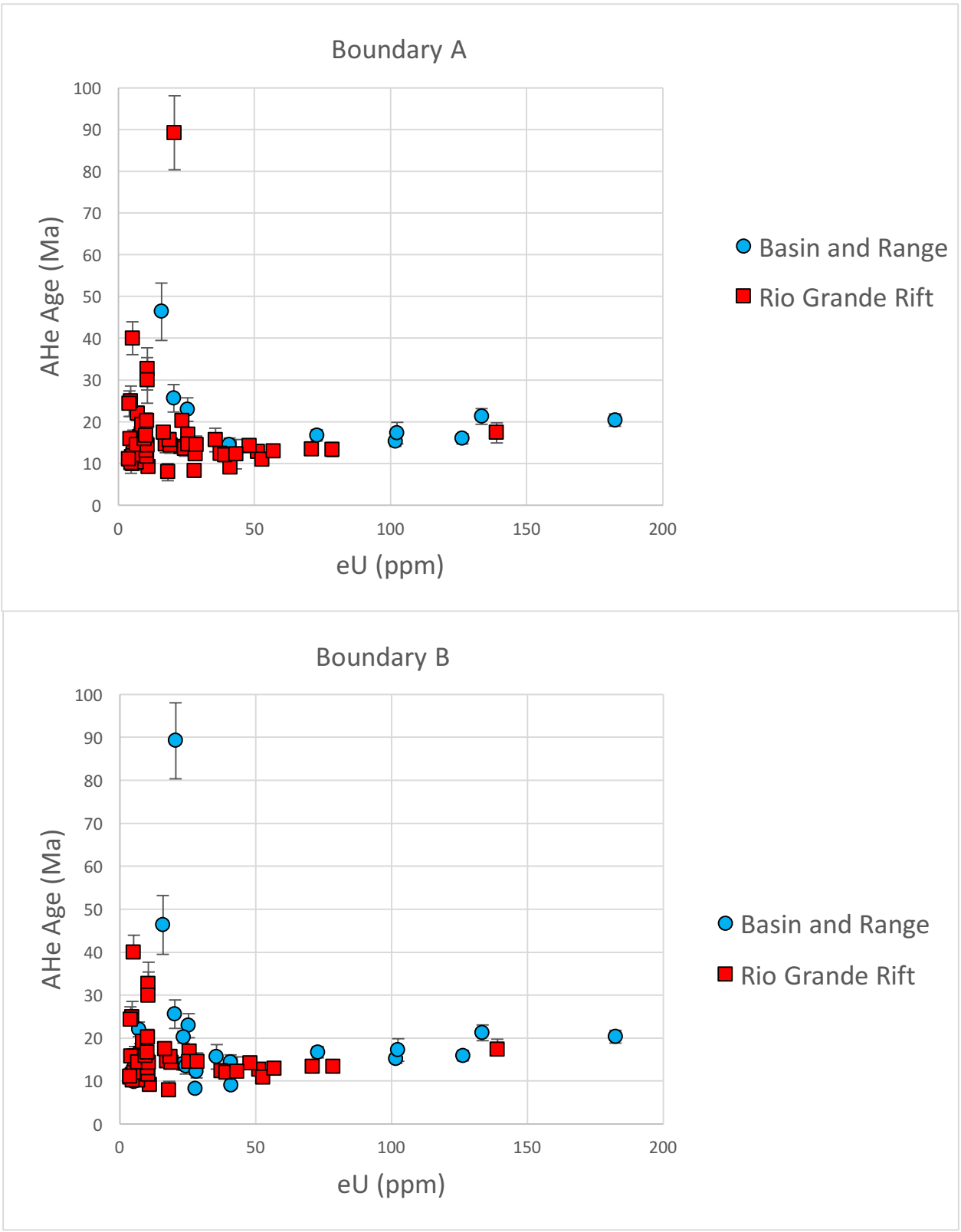

Figure 14: AHe age vs. eU sorted by tectonic province

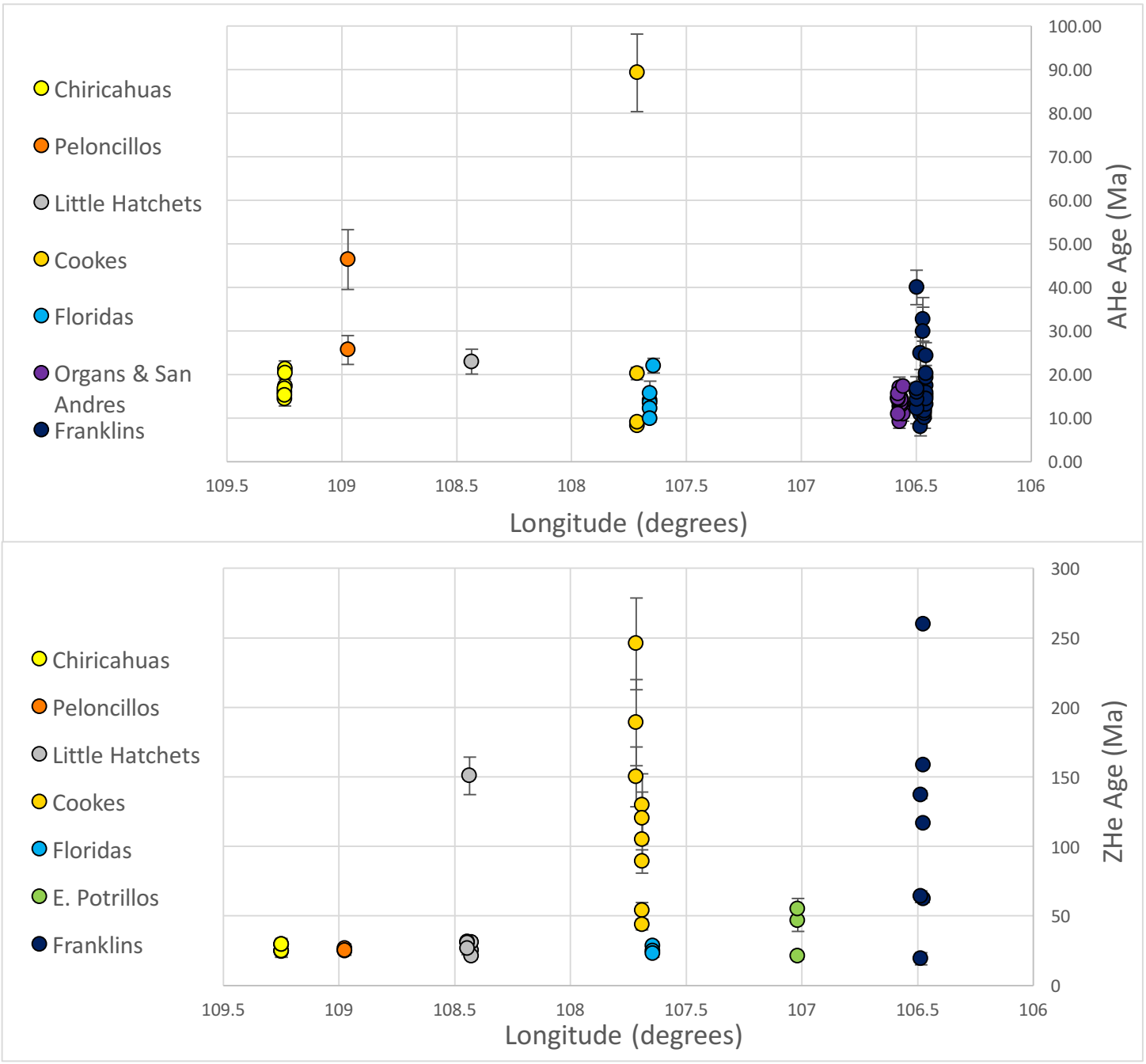

Figure 15: (U-Th)/He ages vs. longitude

ZHe ages from the southern Rio Grande rift show a wide range (19 – 738 Ma), compared to ages from the Basin and Range Province (21 – 31 Ma), using the boundary from Woodward et al. (1978). This relationship suggests that the Rio Grande rift either exhumed samples slowly through the zircon partial retention zone (ZPRZ) or that extension was not sufficient to exhume samples from beneath this temperature window. However, basins in the southern Rio Grande rift are typically deeper, and this region is characterized by higher heat flow, suggesting that samples should have been exhumed from temperatures higher than the ZPRZ. The wide spread in ages cannot be explained by the presence of sedimentary samples (Fig. 16) because although ZHe ages from sedimentary rocks in the Rio Grande rift are generally older, igneous samples from the rift still have older ages as well. Furthermore, 17LH03 was the only sedimentary sample from the Basin and Range and yielded young ZHe ages between 26 and 31 Ma.

Southern Rio Grande rift basins are generally 1 km deep or more, reaching up to 3 km in some places, in contrast to Basin and Range basins, which reach depths < 700 m (Averill and Miller, 2013). Up to 3 km of uplift across the rift is recorded by AFT (Kelly and Chapin, 1997), and the closeness in AHe ages from the southern Rio Grande rift (8 – 40 Ma) and Basin and Range (14 – 46 Ma) suggests that extension in both provinces was sufficient to exhume the ~1-3 km deep apatite PRZ. However, the maximum of 3 km of uplift in the rift is not enough to exhume the > 5 km deep ZPRZ. This implies that ZHe samples from the rift were not exhumed through the ZPRZ, and thus the ages have a wide range. The relatively shallow extensional basins in the Basin and Range suggest that a similar pattern should be seen in their ZHe ages, but the low range of ages means that ZPRZ was exhumed in Basin and Range mountains. This may reflect different structural styles in the Basin and Range and Rio Grande rift. Basin and Range extension is facilitated by listric normal faulting along master detachment faults that exhume deeply-buried

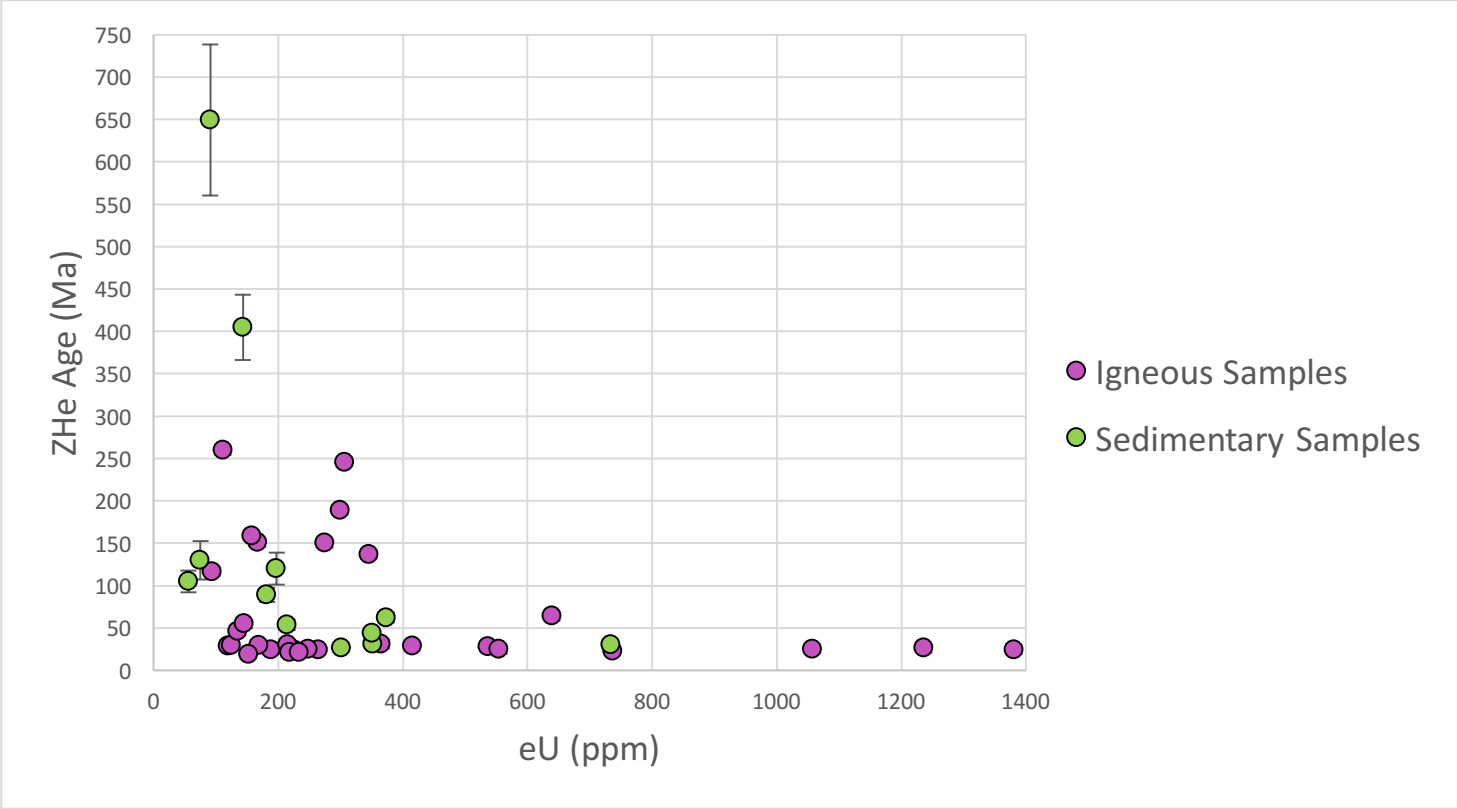

Figure 16: ZHe age vs. eU sorted by sample lithology

rock (Wernicke, 1981; Dickinson, 2002), but create shallow basins. Conversely, the deeper Rio Grande rift basins were formed during late phase rift extension by high angle normal faults that accommodate greater vertical slip (Morgan et al., 1986).

6.2 Comparison of Extensional Styles and Cooling in the Basin and Range and Rio Grande Rift

The difference in structural style between the two provinces predicted by ZHe age vs. eU relationships is supported by seismic imaging across the Basin and Range – Rio Grande rift transition zone in southern New Mexico (Averill, 2007). Sedimentary basins in southern New Mexico are less than 1 km deep but progressively deepen eastward from the Florida Mountains. The seismic reflectivity and velocity patterns in the New Mexico Basin and Range are comparable to that of metamorphic core complex belts in western Arizona and eastern California. The shallow basins and exhumed ZPRZ in the Basin and Range suggest an extension process similar to core complexes, which can exhume deep material with low vertical slip. We propose a master detachment beneath the New Mexico Basin and Range that controlled the uplift of the Chiricahua, Peloncillo, and Little Hatchet Mountains. There exist no detailed seismic surveys of these mountain ranges, so the presence of this hypothesized structure is yet to be tested. However, the large-scale seismic data of the region and patterns of ZHe age vs. eU point towards the existence of this master detachment fault. Furthermore, if the trend of the core complex belt in southern Arizona (Fig. 1) continued eastward, it would cross into southern New Mexico. The similarity between cooling periods of Basin and Range mountains in this study and the period of core complex activity in the Desert Southwest (Fig. 18) also indicates that core complex-style extension may continue into New Mexico.

The cooling periods of mountain ranges in this study as modeled in HeFTy were plotted versus their longitudes to gain insight into patterns of exhumation across the Rio Grande rift-Basin and Range boundary (Fig. 17). As discussed above, there is not a strong constraint on the minimum age of cooling in the Little Hatchets sample 17LH02 but it may be similar to the minimum of ~16 Ma as seen in sample 17LH01. The mountain ranges from the Floridas westward have periods of cooling between 12 and 33 Ma, while the Franklins are the only range showing cooling occurring > 12 Ma. There is not a complete picture of cooling in the study area due to the lack of a Cenozoic cooling model for the East Potrillo Mountains. However, the temporal range of cooling in mountains west of the Franklins is consistent with Basin and Range extension in the Desert Southwest between 30 and 12 Ma.

To further understand the relationship between the studied mountain ranges and the Basin and Range, their cooling periods were plotted with times of extension of metamorphic core complexes (Fig. 18). The cooling of other southern Rio Grande rift mountain ranges outside this study (Sierra Blanca, San Andres Mountains, Organ Mountains; Ricketts et al., 2016) were also compared. The cooling of mountains in the Basin and Range fall within the temporal range of Desert Southwest extension, while the Rio Grande rift mountains have generally younger cooling periods. Cooling in southern rift samples from this study is consistent with the ca. 25-10 Ma period of synchronous extension observed along the entire length of the rift (Ricketts et al., 2016). Samples from Sierra Blanca and the Peloncillo Mountains were collected from plutons that were inferred from their thermal histories to be shallowly emplaced in the crust, and it is likely that they do not record cooling from exhumation (Ricketts et al., 2016; this study).

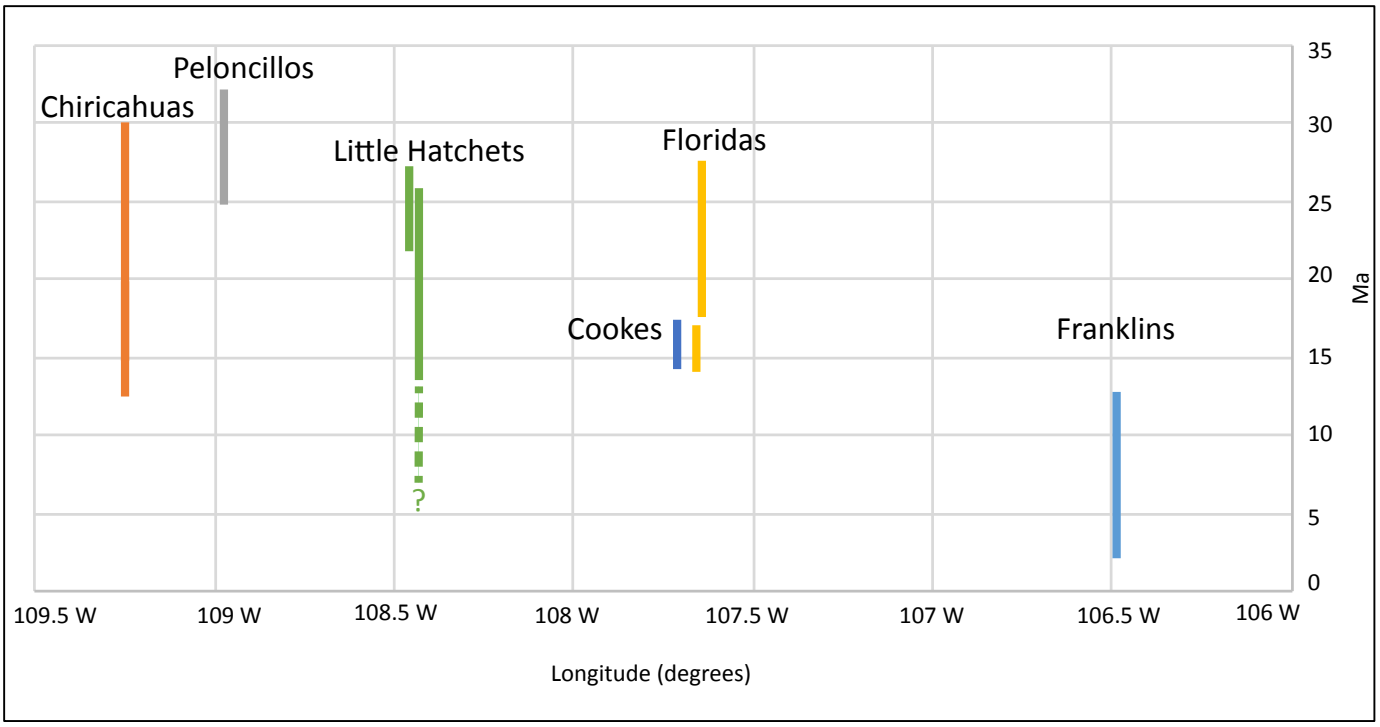

Figure 17: Cooling periods of mountain ranges vs. longitude

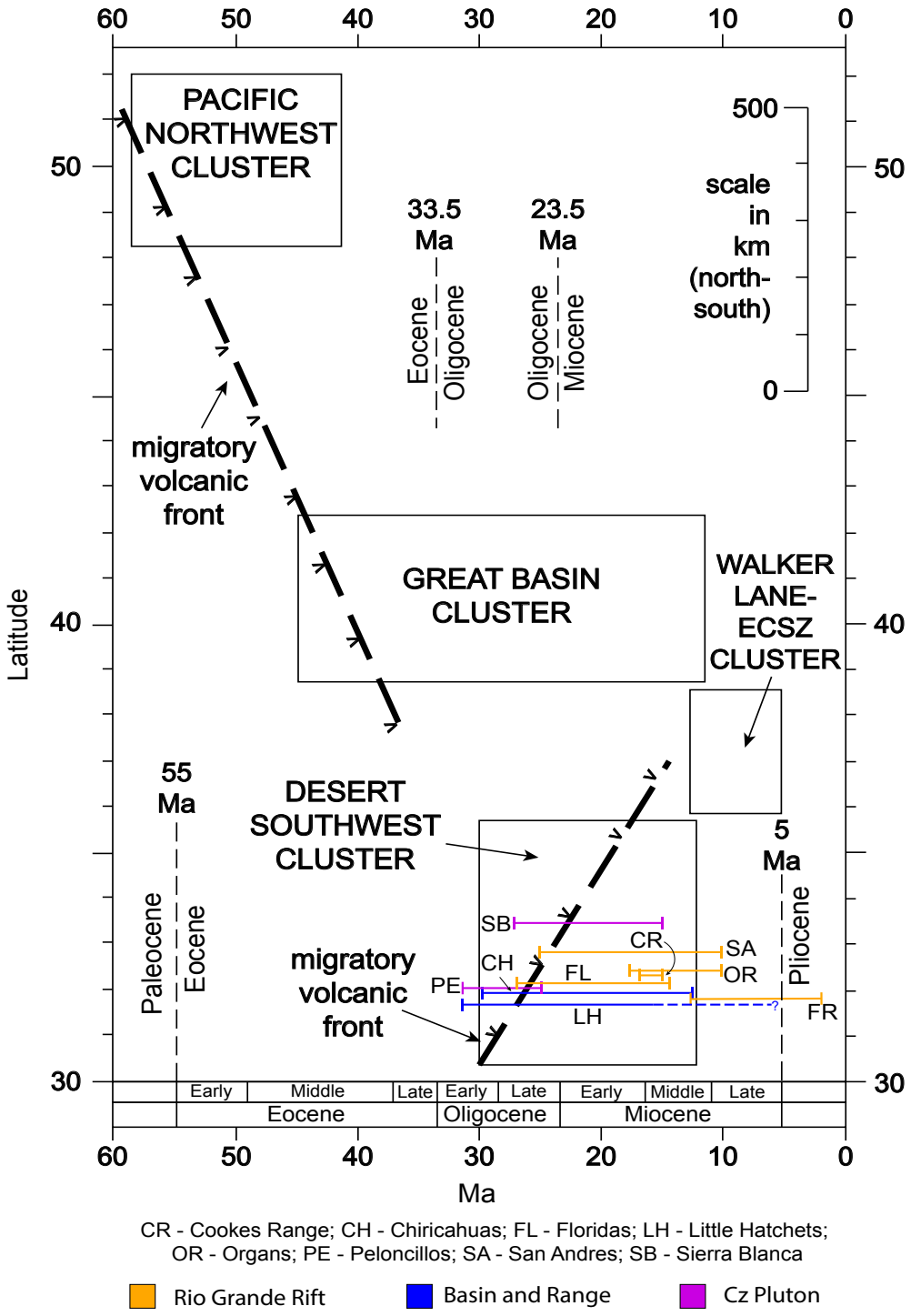

Figure 18: Comparison of extensional periods in the Basin and Range and Rio Grande rift. Boxes represent the spatial and temporal extent of geographic clusters of metamorphic core complexes. Colored lines represent cooling periods of mountain ranges. Figure is modified from Dickinson (2002).

6.3 GEODYNAMIC MODELS FOR THE RIO GRANDE RIFT

Many geodynamic models for the Rio Grande use mantle forces to explain rifting. Seismic imaging of the upper mantle of the Rio Grande rift in central New Mexico shows upwelling mantle beneath the rift axis (West et al., 2004). The upwelling is an inverted U-shaped low velocity anomaly representing relatively cold asthenosphere that has no deep mantle source, but is undergoing small-scale convection. The cold asthenosphere most likely upwelled through advection associated with rifting, and its convection helped drive later extension. Numerical modeling of the thermal development of the rift's lithosphere over time likewise predicts small-scale asthenospheric convection due to lithospheric thinning from rifting (van Wijk et al., 2008). A model involving the foundering of the Farallon plate beneath North America to explain rifting invokes the presence of a slab window in the Farallon that enhanced asthenospheric upwelling and drove extension in the Rio Grande (Ricketts et al., 2016). This model was developed to explain the rift's thin N-S zone of synchronous extension, since the slab window would concentrate mantle convection in a narrow region.

The possibility of a master detachment beneath the Basin and Range in southwestern New Mexico and southeastern Arizona suggests that the simple shear model of extension (Wernicke, 1985) is applicable to the Basin and Range – Rio Grande rift transition (Fig. 19). This model predicts low-angle faulting along a detachment, adjacent to high-angle faulting controlled by higher heat flow under a thinned crust. These features agree with the pattern of ZHe ages and different structural styles of the rift and Basin and Range. The simple shear model is also consistent with the thin crust and upwelling mantle that has been observed beneath the Rio Grande rift.

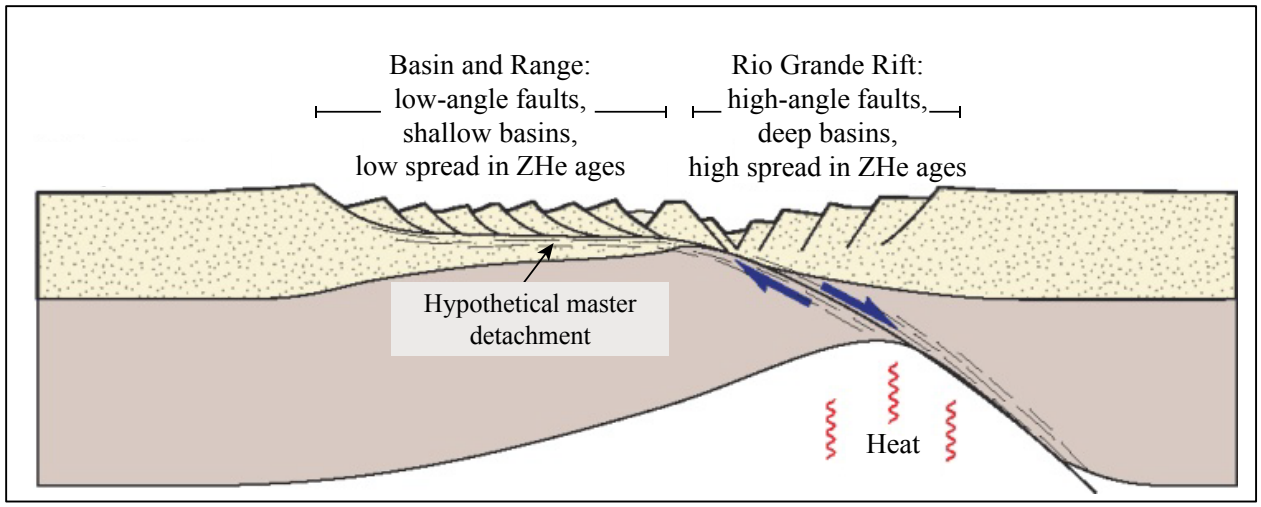

Figure 19: Simple shear model for Basin and Range and Rio Grande rift extension in southern New Mexico. Modified from Fossen (2010).

Chapter 7: Conclusions

A total of 42 new ZHe and 23 new AHe ages were collected from seven mountain ranges across the Rio Grande rift-Basin and Range transition zone in southern New Mexico and Arizona. This data gives new constraints on the times of cooling from each range which are summarized below:

1. ZHe and AHe samples from the Chiricahua and Little Hatchet Mountains in the Basin and Range record cooling between 32 and 16 Ma. This age range coincides with the ca. 30-12.5 Ma period of Basin and Range extension in the Desert Southwest.
2. ZHe and AHe data indicate rapid cooling between ca. 32 and 25 Ma in the Granite Gap pluton from the Peloncillo Mountains. The cooling range is close to the 33.2 Ma age of formation of the rock, indicating that the granite was shallowly emplaced in the crust and cooling is not strongly controlled by rift-related uplift.
3. AHe ages from the Cookes Range document cooling between 16.4 and 12.4 Ma. The relatively high (> 40 Ma) ages from ZHe Cookes Range samples indicate that extension in the range did not uplift the ~5 km deep ZPRZ. ZHe and AHe ages from the Florida Mountains indicate cooling from 27.5-14 Ma. These ranges are located in an ambiguous region between the Basin and Range and the Rio Grande rift, and their times of cooling are consistent with both Desert Southwest extension and the 25-10 Ma period of synchronous extension in the rift. However, ZHe age vs. eU relationships in these ranges imply that extension in these ranges is controlled by the Rio Grande rift.
4. ZHe samples from the East Potrillo Mountains in the Rio Grande rift did not yield any thermal histories that record Cenozoic cooling. This suggests that extension in the Potrillos did not uplift the ZPRZ.

5. ZHe samples from the Franklin Mountains in the Rio Grande rift record cooling between 13 and 2.2 Ma. The times of cooling in the Franklins coincides with the known period of rift-related extension, and agrees with the concept of rifting continuing into the Quaternary.

An abrupt change in ZHe age vs. eU relationships to the west of the Cookes Range and Florida Mountains suggests the presence of a tectonic boundary separating domains with either different extension magnitudes, extension rates, or both. This boundary coincides with the Rio Grande rift – Basin and Range boundary proposed by Woodward et al. (1978). However, more low-temperature thermochronologic data is needed to help constrain times of cooling of mountain ranges in the southern Rio Grande rift, especially in the East Potrillos. Differing extensional styles, crustal thickness, and mantle structure point to a simple shear model of extension across the Basin and Range and Rio Grande rift. The simple shear model suggests a master detachment fault controlling extension in the Chiricahua, Peloncillo, and Little Hatchet Mountains. Detailed seismic surveys of these mountain ranges are needed to investigate the presence of this detachment.

References

Averill, M.G., 2007, A lithospheric investigation of the southern Rio Grande rift [Ph.D. thesis]: University of Texas at El Paso, 231 p.

Averill, M.G., and Miller, K.C., 2013, Upper crustal structure of the southern Rio Grande rift: a composite record of rift and pre-rift tectonics *in* Hudson, M.R. and Grauch, V.J.S., eds., New Perspectives on Rio Grande Rift Basins: From Tectonics to Groundwater, Geological Society of America, Special Paper 494, p. 463-474.

Axen, G.J, Taylor, W.J., and Bartley, J.M., 1993, Space-time patterns and tectonic controls of Tertiary extension and magmatism in the Great Basin of the western United States: geological Society of America Bulletin, v. 105, p. 56-76.

Baldridge, W.S., Olsen, K.H., and Callender, J.F., 1984, Rio Grande rift—Problems and perspectives *in* Baldridge, W. S.; Dickerson, P. W.; Riecker, R. E.; Zidek, J., eds., New Mexico Geological Society 35th Annual Fall Field Conference Guidebook, 379 p.

Baldridge, W.S., Keller, G.R., Haak, V., Wendlandt, E., Jiracek, G.R., and Olsen, K.H., 2006, The Rio Grande rift *in* Olsen, K.H., ed., Continental Rifts: Evolution, Structure, Tectonics: Developments in Geotectonics, v. 25, p. 233-275.

Berglund, H.T., Sheehan, A.F., Murray, M.H., Roy, M., Lowry, A.R., Nerem, R.S., and Blume, F., 2012, Distributed deformation across the Rio Grande rift, Great Plains, and Colorado Plateau: Geology, v. 40, no. 1, p. 23-26.

Bryan, P., and Gordon, R.G., 1990, Rotation of the Colorado Plateau: an updated analysis of paleomagnetic poles: Geophysical Research Letters, v. 17, p. 1501-1504.

Carciumaru, D., and Ortega, R., 2008, Geologic structure of the northern margin of the Chihuahua trough: Evidence for controlled deformation during Laramide Orogeny: Boletín de la Sociedad Geológica Mexicana, v. 60, no. 1, p. 43-69.

Chapin, C.E., and Cather, S.M., 1994, Tectonic setting of axial basins of the northern and central Rio Grande rift, *in* Keller, G.R., and Cather, S.M., eds., Basins of the Rio Grande Rift: Structure, Stratigraphy, and Tectonic Setting: Geological Society of America Special Paper 291, p. 5–25.

Clemons, R.E., 1982, Geology of Massacre Peak quadrangle, Luna county, New Mexico: New Mexico Bureau of Mines & Mineral Resources Geologic Map 51, scale 1:24,000.

Clemons, R.E., 1998, Geology of the Florida Mountains, southwestern New Mexico: New Mexico Bureau of Mines & Mineral Resources Memoir 43, 112 p.

Cordell, L., 1978, Regional geophysical setting of the Rio Grande rift: Geological Society of America Bulletin, v. 89, p. 1073-1090.

Delfin, R.A. and Ricketts, J., 2016, Constraints on the timing of extension in the Franklin Mountains from apatite (U-Th)/He thermochronology, El Paso, Texas: 2016 New Mexico Geological Society Annual Spring Meeting, Socorro, NM, Proceedings Volume, p. 18.

Dickinson, W.R., 2002, The Basin and Range province as a composite extensional domain: International Geology Review, v. 44, p. 1-38.

Dickinson, W.R. and Snyder, W.S., 1979, Geometry of subducted slabs related to San Andreas transform: Journal of Geology, v. 87, p. 609-627.

Drewes, H., du Bray, E.A., and Pallister, J.S., 1995, Geologic map of the Portal quadrangle and vicinity, Cochise County, Arizona: U.S. Geological Survey Miscellaneous Investigations Series Map I-2450, scale 1:24,000.

du Bray, E.A., Pallister, J.S., and Yager, D.B., 1997, Geologic map of the Turkey Creek caldera, Chiricahua Mountains, Cochise County, Arizona: U.S. Geological Survey Miscellaneous Investigations Series Map I-2544, scale 1:50,000, sheet 1.

Eaton, G.P., 1982, The Basin and Range province: origin and tectonic significance: Annual Review of Earth and Planetary Sciences, v. 10, p. 409-440.

Eaton, G.P., 1986, A tectonic redefinition of the southern Rocky Mountains: Tectonophysics, v. 132, p. 163–193.

Fossen, H., 2010, Structural Geology: New York, Cambridge University Press, 480 p.

Flowers, R.M., Ketcham, R.A., Shuster, D.L., and Farley, K.A., 2009, Apatite (U-Th)/He thermochronometry using a radiation damage accumulation and annealing model: Geochimica et Cosmochimica Acta, v. 73, p. 2347-2365.

Gillerman, E., 1958, Geology of the central Peloncillo Mountains, Hidalgo County, New Mexico, and Cochise County, Arizona: New Mexico Bureau of Mines and Mineral Resources Bulletin 57, 170 p.

Goteti, R., Mitra, G., Becene, A., Sussman, A., and Lewis, C., 2013, Three-dimensional finite-element modeling of fault interactions in rift-scale normal fault systems: implications for the late Cenozoic Rio Grande rift of north-central New Mexico *in* Hudson, M.R. and Grauch, V.J.S., eds., New Perspectives on Rio Grande Rift Basins: From Tectonics to Groundwater, Geological Society of America, Special Paper 494, p. 157-184.

Guenthner, W.R., Reiners, P.W., Ketcham, R.A., Nasdala, L., and Giester, G., 2013, Helium diffusion in natural zircon: radiation damage, anisotropy, and the interpretation of zircon (U-Th)/He thermochronology: American Journal of Science, v. 313, p. 145-198.

Hamilton, W., 1981, Plate-tectonic mechanism of Laramide deformation, *in* Boyd, D.W., and Lillegraven, J.A. eds., Rocky Mountain Foreland Basement Tectonics: University of Wyoming Contributions to Geology, v. 19, p. 87–92.

Harbour, R.L., 1972, Geology of the northern Franklin Mountains, Texas and New Mexico, Geological Survey Bulletin 1298, 138 p.

Harrison, T.M. and Zeitler, P.K., 2005, Fundamentals of noble gas thermochronometry *in* Reiners, P.W. and Ehlers T.A., eds., Low Temperature Thermochronology: Techniques, Interpretations, and Applications: Mineralogical Society of America, Reviews in Mineralogy and Geochemistry, v. 58, p. 123-149.

House, M.A., Kelley, S.A., and Roy, M., 2003, Refining the footwall cooling history of a rift flank uplift, Rio Grande rift, New Mexico: Tectonics, v. 22., no. 5, p. 1-18.

Humphreys, E., 2009, Relation of flat slab subduction to magmatism and deformation in the western United States, *in* Kay, S.M., Ramos, V.A., and Dickinson, W.R., eds., Backbone of the Americas: Shallow Subduction, Plateau Uplift, and Ridge and Terrane Collision: Geological Society of America Memoir 204, p. 85–98

Johnson, J.E., Flowers, R.M., Baird, G.B., and Mahan, K.H., 2017, "Inverted" zircon and apatite (U-Th)/He dates from the Front Range, Colorado: High-damage zircon as a low-temperature (<50 °C) thermochronometer: Earth and Planetary Science Letters, v. 466, pg. 80-90.

Ketcham, R.A., 2005, Forward and inverse modeling of low-temperature thermochronometry data *in* Reiners, P.W. and Ehlers T.A., eds., Low Temperature Thermochronology: Techniques, Interpretations, and Applications: Mineralogical Society of America, Reviews in Mineralogy and Geochemistry, v. 58, p. 275-314.

Keller, G.R., Morgan, P., and Seager, W.R., 1990, Crustal structure, gravity anomalies and heat flow in the southern Rio Grande rift and their relationship to extensional tectonics: Tectonophysics, v. 174, p. 21–37.
Kelley, S. and Chamberlin, R., 2012, Our growing understanding of the Rio Grande rift: New Mexico Earth Matters, v. 12, no. 2, 5 p.
Kelley, S.A., and Chapin, C.E., 1997, Cooling histories of mountain ranges in the southern Rio Grande rift based on apatite fission-track analysis – a reconnaissance survey: New Mexico Geology, v. 19, no. 1, p. 1-14.
Kelley, S.A., Chapin, C.E., and Corrigan, J., 1992, Late Mesozoic to Cenozoic cooling histories of the flanks of the northern and central Rio Grande rift, Colorado and New Mexico: New Mexico Bureau of Mines and Mineral Resources Bulletin 145, 39 p.
Kelley, V.C., 1952, Tectonics of the Rio Grande depression of central New Mexico, *in* Johnson, R.B., and Read. C.B., eds. Rio Grande Country: New Mexico Geological Society Guidebook 3, p. 92-105.
Ketcham, R.A., Gautheron, C., and Tassan-Got, L., 2011, Accounting for long alpha-particle stopping distance in (U-Th-Sm)/He geochronology: refinement of the baseline case: Geochemica et Cosmochimica Acta, v. 75, p. 7779-7791.
Landman, R.L., and Flowers, R.M., 2013, (U-Th)/He thermochronologic constraints on the evolution of the northern Rio Grande Rift, Gore Range, Colorado, and implications for rift propagation models: Geosphere, v. 9, p. 170-187.
Long, K.B., Baldwin, S.L., and Gehrels, G.E., 1995, Tectonothermal evolution of the Pinaleño-Jackson Mountain core complex, southeast Arizona: GSA Bulletin, v. 107, p. 1231-1240.
Lovejoy, E.M.P., 1975, An interpretation of the structural geology of the Franklin Mountains, Texas, *in* Seager, W.R., Clemons, R.E., and Callender, J.F., eds., Las Cruces Country: New Mexico Geological Society Annual Fall Field Conference Guidebook, 26th, 376 p.
Machette, M.N., 1987, Preliminary assessment of paleoseismicity at White Sands Missile Range, southern New Mexico: Evidence for recency of faulting, fault segmentation, and repeat intervals for major earthquakes in the region: U.S. Geological Survey Open-File Report 87-444, 49 p.
Mack, G.H., 2004, Middle and late Cenozoic crustal extension, sedimentation, and volcanism in the southern Rio Grande rift, Basin and Range, and southern transition zone of southwestern New Mexico, *in* Mack, G.H., and Giles, K.A., eds., The Geology of New Mexico, A Geologic History: New Mexico Geological Society Special Publication 11, p. 389–406.
McLemore, V.T., McIntosh, W.C., and Pease, T.C., 1995, 40Ar/39Ar age determinations of four plutons associated with mineral deposits in southwestern New Mexico: New Mexico Bureau of Mines and Mineral Resources Openfile Report 410, 36 p.
McLemore, V.T., Heinonen, A., Rämö, T., Andersen, T., and Mäntärri, I., 2012, 1100 Ma rapakivi granites, Little Hatchet Mountains, southwestern New Mexico: Geological Society of America Abstracts with Programs, v. 44, no. 6, p. 9.
Morgan, P., Seager, W.R., and Golombek, M.P., 1986, Cenozoic thermal, mechanical and tectonic evolution of the Rio Grande rift: Journal of Geophysical Research, v. 91, p. 6263-6276.
Moucha, R., Forte, A.M., Rowley, D.B., Mitrovica, J.X., Simmons, N.A., and Grand, S.P., 2008, Mantle convection and the recent evolution of the Colorado Plateau and the Rio Grande rift valley: Geology, v. 36, p. 439-442.

Nicholson, C., Sorlien, C.C., Atwater, T., Crowell, J.C., and Luyendyk, B.P., 1992, Microplate capture, rotation of the western Transverse Ranges, and initiation of the San Andreas transform as a low-angle fault system: Geology, v. 22, p. 491-495.

Reiners, P.W., 2005, Zircon (U-Th)/He thermochronometry *in* Reiners, P.W. and Ehlers T.A., eds., Low Temperature Thermochronology: Techniques, Interpretations, and Applications: Mineralogical Society of America, Reviews in Mineralogy and Geochemistry, v. 58, p. 151-179.

Ricketts, J.W., Karlstrom, K.E., and Kelley, S.A., 2015, Embryonic core complexes in narrow continental rifts: the importance of low-angle normal faults in the Rio Grande rift of central New Mexico: Geosphere, v. 11, no. 2, p. 425-444.

Ricketts, J.W., Kelley, S.A., Karlstrom, K.E., Schmandt, B., Donahue, M.S., and van Wijk, J., 2016, Synchronous opening of the Rio Grande rift along its entire length at 25-10 Ma supported by apatite (U-Th)/He and fission-track thermochronology, and evaluation of possible driving mechanisms: Geological Society of America Bulletin, v. 128, no. 3, p. 397–424.

Seager, W.R., and Mack, G.H., 1994, Geology of East Potrillo Mountains and vicinity, Doña Ana County, New Mexico: New Mexico Bureau of Mines and Mineral Resources Bulletin 113, 27 p.

Seager, W.R., and Morgan, P., 1979, Rio Grande rift in southern New Mexico, west Texas, and northern Chihuahua, *in* Riecker, R.E., ed., Rio Grande Rift: Tectonics and Magmatism: Washington, D.C., American Geophysical Union, p. 87–106.

Shannon, W.M., Barnes, C.G., and Bickford, M.E., 1997, Grenville magmatism in west Texas: petrology and geochemistry of the Red Bluff granitic suite: Journal of Petrology, v. 38, no. 10, p. 1279-1305.

Staude, J.G., and Barton, M.D., 2001, Jurassic to Holocene tectonics, magmatism, and metallogeny of northwestern Mexico: GSA Bulletin, v. 113, no. 10, p. 1357-1374.

Stock, J.M., and Hodges, K.V., 1989, Pre-Pliocene extension around the Gulf of California and the transfer of Baja California to the Pacific plate: Tectonics, v. 8, p. 99-115.

Stockli, D.F., 2005, Application of low-temperature thermochronometry to extensional tectonic settings *in* Reiners, P.W. and Ehlers T.A., eds., Low Temperature Thermochronology: Techniques, Interpretations, and Applications: Mineralogical Society of America, Reviews in Mineralogy and Geochemistry, v. 58, p. 411-448.

Tagami, T. and O'Sullivan, P.B., 2005, Fundamentals of fission-track thermochronology *in* Reiners, P.W. and Ehlers T.A., eds., Low Temperature Thermochronology: Techniques, Interpretations, and Applications: Mineralogical Society of America, Reviews in Mineralogy and Geochemistry, v. 58, p. 19-47.

van Wijk, J., van Hunen, J., and Goes, S., 2008, Small-scale convection during continental rifting: Evidence from the Rio Grande rift: Geology, v. 36, p. 575–578.

Vermeesch, P., and Tian, Y., 2014, Thermal history modelling; HeFTy vs. QTQt: Earth-Science Reviews, v. 139, p. 279-290.

Wernicke, B., 1981, Low-angle normal faults in the Basin and Range Province: nappe tectonics in an extending orogen: Nature, v. 291, p. 645-648.

Wernicke, B., 1985, Uniform-sense normal simple shear of the continental lithosphere: Canadian Journal of Earth Sciences, v. 22, no. 1, p. 108-125.

West, M., Ni, J., Baldridge, W.S., Wilson, D., Aster, R., Gao, W., and Grand, S., 2004, Crust and upper mantle shear wave structure of the southwest United States: implications for rifting and support for high elevation: Journal of Geophysical Research, v. 109, B03309.

Woodward, L.A., Callender, J.F., Seager, W.R>, Chapin, C.E., Gries, J.C., Shaffer, W. L., and Zilinski, R.E., 1978, Tectonic map of Rio Grande rift region in New Mexico, Chihuahua, and Texas: New Mexico Bureau of Mines and Mineral Resources, Circular 163, scale 1:1,000,000, sheet 2.

Zeller, R.A., Jr., 1970, Geology of the Little Hatchet Mountains, Hidalgo and Grant Counties, New Mexico: New Mexico Bureau of Mines and Mineral Resources Bulletin 96, 33 p.

Vita

Julian Malachy Biddle was born in 1995 in El Paso, Texas. He attended high school in El Paso at Transmountain Early College High School, where he earned an Associate of Arts along with his high school diploma in 2012. He began studying geology at the Geological Sciences Department at the University of Texas at El Paso (UTEP), and received his Bachelor of Science in Geology in 2015. He was accepted the following year to the geology Master's program at UTEP. Julian received his Master of Science in Geology in 2017.

Contact Information: <jmbiddle@miners.utep.edu>

This thesis was typed by Julian Malachy Biddle